THE UNIVERSITY OF CHICAGO

SIMULTANEOUS TARGETING OF MULTIPLE CANCER-SPECIFIC ANTIGENS ON A CANCER CELL BY ONE CHIMERIC ANTIGEN RECEPTOR

A DISSERTATION SUBMITTED TO

THE FACULTY OF THE DIVISION OF THE BIOLOGICAL SCIENCES

AND THE PRITZKER SCHOOL OF MEDICINE

IN CANDIDACY FOR THE DEGREE OF

DOCTOR OF PHILOSOPHY

COMMITTEE ON CANCER BIOLOGY

BY

YANRAN HE

CHICAGO, ILLINOIS

AUGUST 2019

TABLE OF CONTENTS

LIST OF TABLES

LIST OF FIGURES

LIST OF ABBREVIATIONS

2A, self-cleaving 2A peptide

'T' in T2A, *Thosea asigna* virus

'P' in P2A, porcine teschovirus-1

aa, amino acid

Ab, antibody

ACT, adoptive T-cell transfer

Ag, antigen

Ala, alanine

ALV, antigen loss variant

Asn, asparagine

B6, C57BL/6

CAR, chimeric antigen receptor

CBGluc, click beetle green luciferase

CD, cluster of differentiation

core 1 β3GalT, core 1 β1,3-galactosyltransferase

core 3 β3GlcNAcT, core 3 β1,3-N- acetylglucosaminyltransferase

COSMC, core 1 β3 galactosyltransferase-specific molecular chaperone

EGFP, enhanced green fluorescent protein

EVI2B, protein EVI2B

GalNAc, *N*-acetylgalactosamine

GlcNAc, *N*-acetylglucosamine

HLA, human leukocyte antigen

IL-2, interleukin 2

IRES, internal ribosome entry site

i.p., intraperitoneal(ly)

i.v., intraveneous(ly)

LAMP, lysosome-associated membrane glycoprotein 1

MACS, magnetic-activated cell sorting

MFI, median fluorescence intensity

MHC, major histocompatibility complex

MUC1, mucin 1

NSG, NOD.Cg-Prkdc^{scid} Il2rg^{tm1Wjl}/SzJ

OT-I, ovalbumin-specific, CD8+ T-cells

PCDH9, protocadherin-9

PDPN, podoplanin

PDXL, podocalyxin-like protein 2

ppGalNAcT: *N*-acetylgalactosaminyltransferase

PTM, post-translational modification

Rag1, recombination activating gene 1

RBC, red blood cell

r/r, refractory / relapsed

RT, room temperature

SB, staining buffer

s.c., subcutaneous injection

scFv, single chain variable fragment

Ser, serine

SoC, standard of care

TAA, tumor associated antigens

TCGA, The Cancer Genome Atlas

TCR, T-cell receptor

TCRT, TCR-engineered T-cell

TFRC, transferrin receptor protein 1

thCD19, truncated human CD19

Thr, threonine

TIL, tumor infiltrating lymphocytes

Tn, “T antigen nouvelle”

TSA, tumor specific antigens

ZIP6, zinc transporter ZIP6

ACKNOWLEDGMENTS

I would like to thank my advisor, Dr. Hans Schreiber, for giving me much guidance in research and in life. He and Ms. Karin Schreiber are the epitomes of commitment and diligence, handle ridiculous hardship with such benevolence and grace. I always will be encouraged by Hans's wisdom of " You have to work really hard to be lucky" and I hope I can embrace future challenges with similar thoughtfulness and perseverance like the Schreibers.

I would like to thank the wonderful members of my thesis committee and everyone who has provided me with invaluable help throughout my study. Specially, I would like to thank Dr. Jun Huang for leading me into the world of microscopic imaging that allows me to examine immunological processes dynamically at the molecular level. I would also like to thank Dr. Stephen Meredith and Dr. Erin Adams for broadening my horizons by gaining insights about the structural basis of biological events. My appreciation goes to Dr. David Kranz and Dr. H. Michael Shepard, for inspiring me to identify multiple different natural antigens in a cancer cell, on top of many generous helps that I have received from them. Moreover, I would like to express much gratitude to Dr. Michael Spiotto and Dr. Yang-Xin Fu, for taking their precious time to provide me with very informative and constructive suggestions. Many thanks to Dr. Bernard Roizman for bringing me to this incredible adventure. Last but not least, Dr. Janet Rowley for helping me get through an especially challenging time.

I am privileged to have had the opportunity to collaborate with many brilliant minds. I would like to express my gratitude to Dr. Preeti Sharma and Dr. Qi Cai from Dr. David Kranz's lab; Dr. Jonathan Zerweck, Dr. Adam Gasser and Patrick Moore from Dr. Stephen Meredith's lab. Dr. Dibyendu Sasmal, Dr. Wei Feng, Guoshuai Cao, Yifei Hu, Jillian Rosenberg, Laura Pulido from

Dr. Jun Huang's lab. Dr. Sobhan Roy from Dr. Erin Adams lab for the wonderful opportunity of working together and learning from them.

I thank members of the Schreiber's lab, past and present. Especially Steven Wolf and Paula Böttinger for being the best labmate one could ever ask for and for being my Leidensgenosse. I would like to thank Dr. Frank Wen, for his good company in commiserating about our situations. I am profoundly thankful to Dr. Christian Idel, for helping me get started in Schreiberia when everything looked so confusing and intimidating. A shout out to Ms. Madeline Steiner, Ms. Jessie Bronski, Ms. Elizabeth Jensen and Ms. Cecelia Lai for taking good care of the lab.

I feel indebted to my family for their understanding and unconditional support that allows me to focus on my study. The past half a year has been an especially challenging time for everyone in the family in the face of my father's illness. But we stay strong together.

Last but not least, I would like to thank Dr. Danxia Xie for always believe in me more than I could have imagined for myself, for his unyielding support in driving me to fulfill my commitments and goals, for sharing a similar view of the world and so deeply passionate about turning it into a better place for our future generations. I am a lucky one in 7.5 billion to find my soulmate and better half during my time at the University of Chicago.

I am very fortunate to not only complete my graduate study here in Chicago but also run into the most wonderful group of people in my life, without whom I wouldn't be able to stand where I am today. My forever gratitude to all of my amazing colleagues, friends and family, with your blessing I have gained much courage to face whatever course my life will take with much confidence and grace.

1. INTRODUCTION

1.1. Adoptive T-cell transfer for cancer therapy

Adoptive T-cell transfer (ACT) is a class of cancer treatment using adoptively transferred T cells to mediate tumor regression *in vivo*. The earliest attempt in this class was to give patients autologous tumor infiltrating lymphocytes (TIL) followed by systematic IL-2 administration to boost the T-cell transfer. TIL therapy has emerged as one of the most effective treatment for refractory/relapsed (r/r) cancer patients across multiple solid cancer types (1-4). Nevertheless, the broader application of TIL therapy is significantly limited by 3 factors: a) the time and cost to prepare autologous TILs for each individual patient b) the heterogeneity of the percentage of tumor reactive T cells in TILs from different patients c) the toxicity of systematically administered IL-2 that may lead to treatment discontinuation (5).

With the advancement of gene editing technology especially in the past decade, it has become increasingly feasible to transduce T cells with a T-cell receptor (TCR) of known tumor reactivity (6, 7). The TCR-engineered T-cell (TCRT) improves upon the previous TIL therapy by ensuring T cells with defined cancer-reactivity. However, cancer cells can still circumvent recognition by TCRT cells either via the loss of antigen expression, or down-regulation of the MHC responsible for the presentation of the epitope (8). Moreover, TCRT cannot recognize surface antigens that are not being presented on MHCs like CD19.

Chimeric antigen receptors (CAR) are artificial receptors that combine the single chain variable fragment (*scFv*) of a monoclonal antibody (mAb) and the T-cell-activating signals (**Figure 1**). It combines the specificity of a mAb recognizing cell surface antigens independent of MHC presentation, and the efficacy of effector T cells. The 1st generation CAR is a fusion of a *scFv* of an Ab to a CD3ζ of a TCR complex. CD3ζ aggregation upon *scFv* binding induced

target lysis by activated T cells (9). However, the 1st generation CART was susceptible to T-cell exhaustion and failed to achieve durable responses *in vivo*. The 2nd generation CAR integrated a T-cell co-stimulatory signal in tandem with CD3ζ, which significantly improved the potency and persistence of CART cells both *in vitro* and *in vivo* (10). CART treatment has attracted much attention due to its independence of MHC presentation, the capability to target a wide range of cell surface antigens, and the significant efficacy in treating late-stage leukemia patients by targeting a B-cell lineage marker CD19 (11). However, the broader application of CART beyond its success in treating B cell leukemia has been severely limited by a) the small number of cell surface antigens that are cancer-specific and widely and stably expressed by the cancer cells b) the severe toxicities caused by on-target, off-tumor recognition of the antigens expressed on the normal tissues (12), b) cancer relapses from antigen-loss-variants (13-16).

To this end, my graduate work is dedicated to overcoming these abovementioned issues by simultaneously targeting multiple cancer-specific antigens to avoid toxicity while minimizing the risks of relapses from antigen-loss-variants (ALVs)

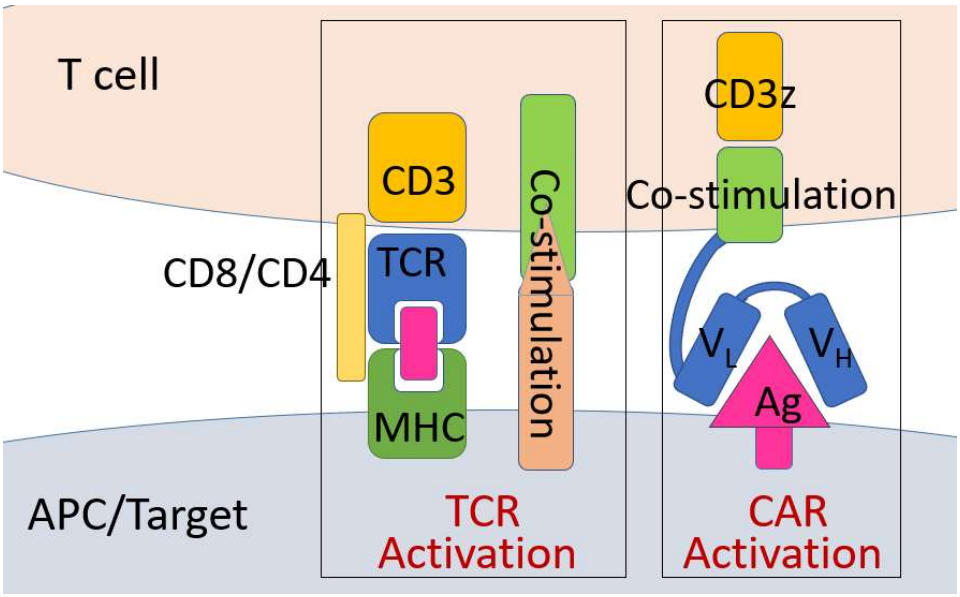

Figure 1. The schematic diagram of T-cell activation through TCR or CAR recognition. TCRs recognize peptide antigens presented on MHCs by the TCRs. CARs recognize cell surface Ags by their extracellular *scFv*. CARs mimic T-cell signaling upon TCR engagement by adopting CD3ζ and TCR co-signaling components as their intracellular signaling domain.

1.2 Aberrant glycosylation in cancers

Glycosylation is one of the most important post-translational modifications (PTM) for proteins. Glycoproteins play various functions in normal and pathological biological processes. The two main types of glycosylation in mammalian cells are *N*-linked glycosylation of a GlcNAc linked to the nitrogen of an Asn; and the *O*-linked glycosylation that are glycans linked to the Ser/Thr residues through the connection of a GalNAc to the C6 hydroxy group.

Glycosylation is a complicated process and the proper elongation of glycans relies on the normal function of numerous different glycotransferases. Hypoglycosylation is a common feature in cancers due to various defects that could happen during the normal glycosylation process (**Figure 2**). Disrupted glycosylation generates a novel class of tumor-associated antigens that are known as the tumor-associated carbohydrate antigen (TACA) (reviewed in (17). TACAs are attractive targets for cancer immunotherapy due to their prevalence and cancer-specificity. Nevertheless, regardless of several decades of efforts to develop cancer vaccines targeting TACAs, very limited clinical success has been achieved. One of the critical issues is that carbohydrate antigens alone would not induce sufficient immunogenicity to eliminate established cancers (18). Carbohydrate antigens normally only induce weak IgM humoral responses, the affinity of which is very poor, and the Ab is generally not sufficient for therapeutic purposes. Using glycopeptides rather than the carbohydrate moiety alone has successfully induced class switching and elicited IgG rather than IgM responses (19), providing a promising approach to generate high affinity Abs for targeting TACA antigens.

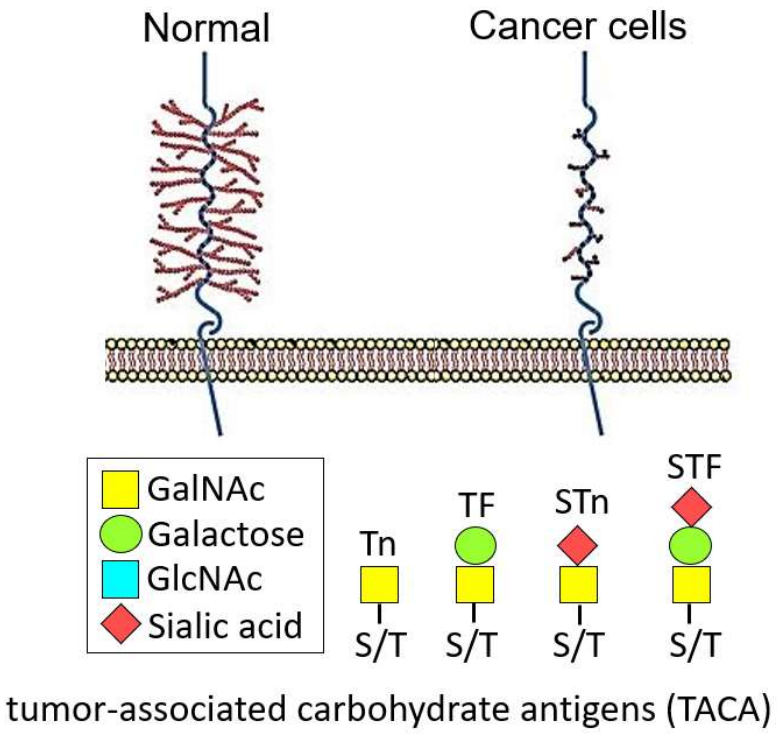

Figure 2. Hypoglycosylation of surface proteins is a common feature of cancer cells. Common types of tumor-associated carbohydrate antigens (TACA) that result from cancer-specific or cancer-associated genetic/epigenetic changes. (The top panel is modified from Fig. 1 in Roulois, D, *et al*. *BioMed research international* (2013) (20))

1.3 Tn-glycopeptides as attractive cancer-specific targets

Over 10% of human proteins are *O*-linked glycoproteins (21). The *O*-linked GalNAc to the Ser/Thr residues is the common precursor of all *O*-linked glycopeptides and it is called Tn (22). The formation of Tn in the Golgi is mediated by at least 24 different *N*-acetylgalactosaminyltransferases (ppGalNAcTs) in human, each recognizing a different but possibly partially overlapping peptide sequence and catalyzing the addition of GalNAc to the Ser/Thr residues in the peptide sequence (23-26).

In normal tissue, Tn acts as the receptor for galactose in the Golgi catalyzed by glycoprotein-N-acetylgalactosamine 3-β-galactosyltransferase, also known as C1GALT1, in the Golgi to form the Core 1 structure (T antigen). Therefore, C1GALT1 is also called as Core 1 synthase or T synthase. The glycan elongation following the formation of Tn in the Golgi apparatus happens so fast that Tn is not observed in normal tissue even with intracellular staining (27-29).

Remarkably, there is only one functional gene for T-synthase in human, and the correct folding of T-synthase requires one and the only dedicated chaperone, the Core 1 β3 galactosyltransferase-specific molecular chaperone, COSMC (30).

Genetic and epigenetic abnormalities in the steps following the formation of Tn could result in truncated glycosylation that exposes Tn epitope on *O*-linked glycoproteins which is not present under normal physiological conditions. Known mechanisms that contribute to Tn-glycosylation include loss-of-function mutation of either COSMC or T synthase (30, 31), the frequency and the types of which are displayed in **Figure 3** and **Figure 4**. In addition, altered expression or localization of different types of ppGalNacTs can lead to Tn-glycosylation as well (32-37). Epigenetic silencing of COSMC and/or T-synthase expression is another

mechanism that may result in stable Tn expression (38, 39). Surface Tn expression has only been described in cancers as described above, or in a rare type of hemolytic anemia called Tn syndrome that result from either the somatic mutation of *COSMC* or hypermethylation of the promoter region (40-42). The absence of Tn under normal physiological conditions makes Tn-glycopeptides desirables targets for cancer treatment.

In order to identify patients whose cancers have surface Tn-glycosylation that could serve as antigens for targeted therapies, a combined approach of genetic testing and Ab staining is recommended. Detecting surface Tn expression using Tn-specific Ab measured by flow cytometry would be ideal for determining surface Tn expression. However, it is challenging to acquire cells for flow cytometry directly from biopsies. IHC would be more applicable under clinical settings, however it would not be possible or at least challenging for clinicians to differentiate the samples with surface expression from the ones that only have Tn intracellularly. Detecting functional transcripts of COSMC and T-synthase would be complementary to IHC. Although the tests would be dependent on the quality of RNAs and interpretation of missense mutations that might only be partially comprising rather than completely abandoning the function of the genes. Furthermore, genomic sequencing of COSMC and T-synthase genes would provide additional information about the mutations in the UTR and intron regions, which could modulate the expression level of the gene products. As it has been noted above, epigenetic modulations could also contribute to Tn-expression(38), which can be captured by surface Tn staining or examining the methylation status of the promoter region of genes coding for COSMC or T-synthase.

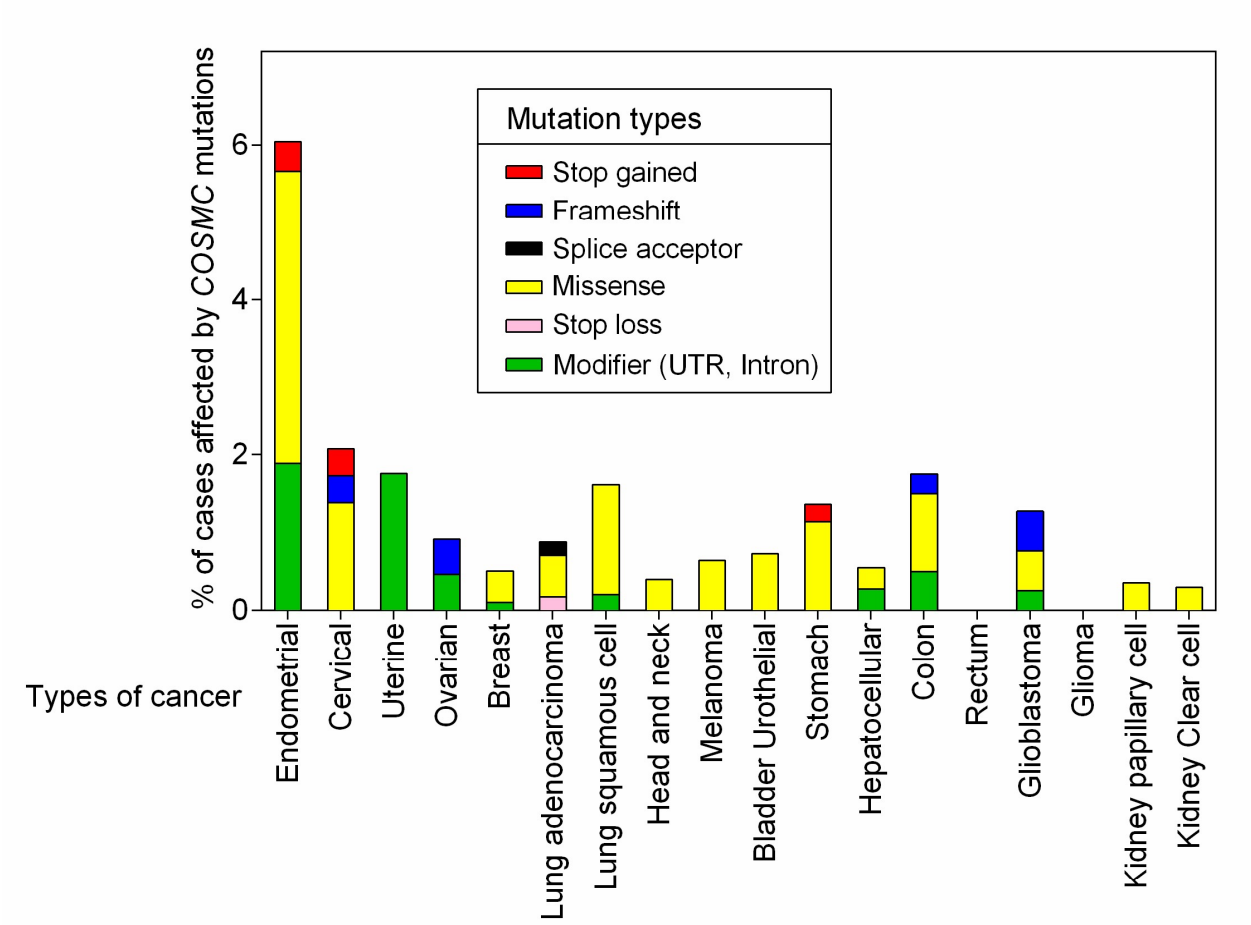

Mutations	35	6	1	4	5	5	8	2	3	3	6	2	7	0	5	0	1	1
Cases affected	30	6	1	4	5	5	8	2	3	3	6	2	7	0	5	0	1	1
Total cases	530	289	57	436	986	567	495	508	469	412	440	364	400	137	393	510	281	336

Figure 3. The frequency of different types of COSMC mutations across cancer types (excluding synonymous mutations). Data were extracted from The Cancer Genome Atlas database (https://portal.gdc.cancer.gov). The different types of mutations are indicated as that in the figure legend. The number of mutations, cases affected and total number of cases in each database of different types of cancers are shown in the bottom.

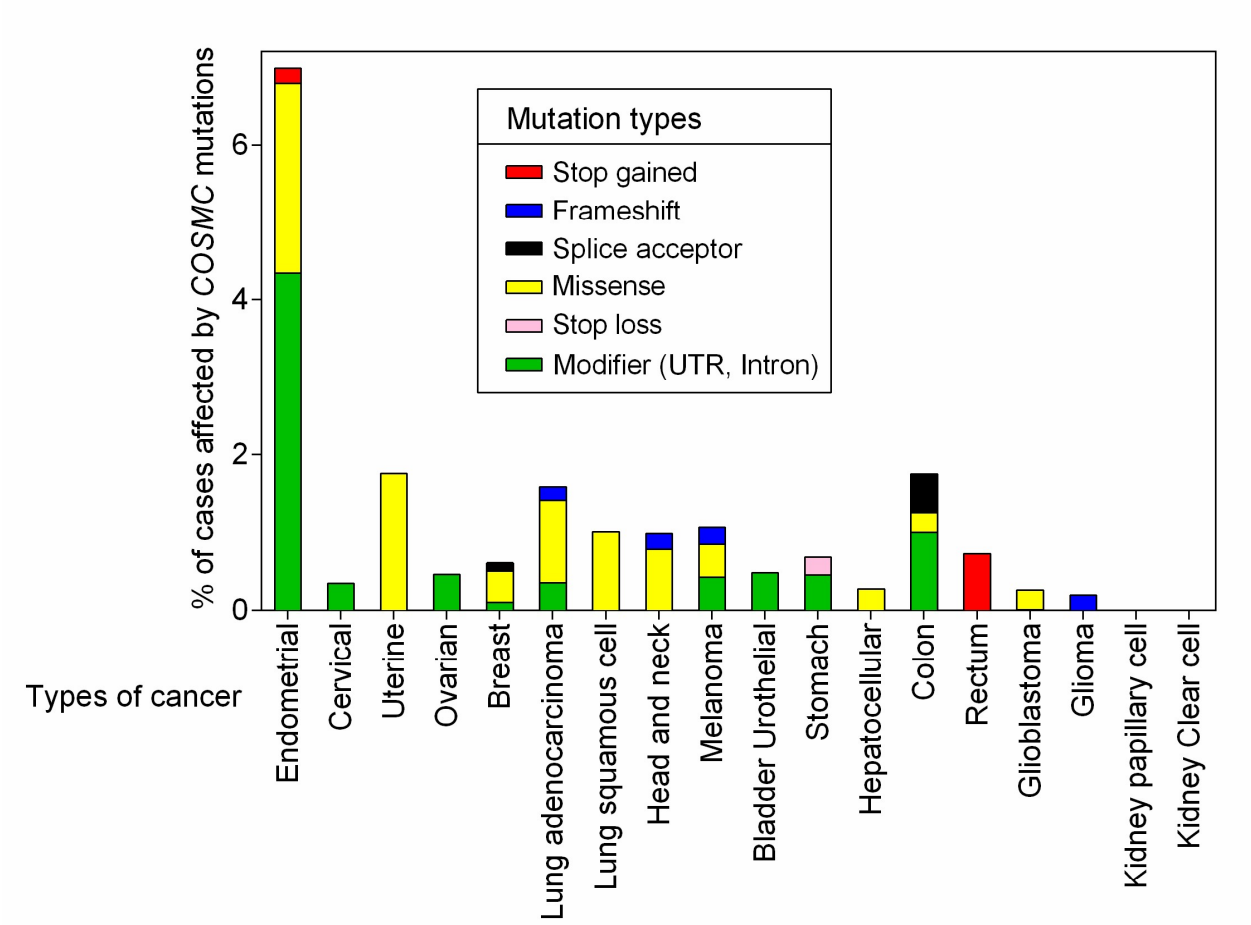

Mutations	34	1	1	2	7	10	5	6	10	3	5	1	10	1	3	1	0	0
Cases affected	25	1	1	2	6	9	5	6	8	2	3	1	7	1	3	1	0	0
Total cases	530	289	57	436	986	567	495	508	469	412	440	364	400	137	393	510	281	336

Figure 4. The frequency of different types of T-synthase mutations across cancer types (excluding synonymous mutations). Data were extracted from The Cancer Genome Atlas database (https://portal.gdc.cancer.gov). The different types of mutations are indicated as that in the figure legend. The number of mutations, cases affected and total number of cases in each database of different types of cancers are shown in the bottom.

1.4 Targeting a Tn-glycopeptide epitope with the 237 monoclonal Ab

237 is an IgG2a monoclonal Ab (237Ab) generated from a mouse simultaneously bearing two spontaneous sarcomas Ag104A and Ag104B in different locations (43). 237Ab specifically recognizes Ag104A but not Ag104B nor the heart/lung/fibroblast (HLF) developed from normal tissues of the same mouse (43). Later research identified that tumor Ag104A carries a somatic in-frame deletion mutation of *Cosmc*, whereby truncating 26 aa residues in the C-terminal region of the extracellular domain and abolishing normal COSMC function, while Ag104B has normal wildtype *Cosmc* gene and functional COSMC (44). Previous research has determined that 237Ab specifically recognizes an epitope surrounding the Tn-glycosylated Thr^{77} of murine podoplanin (mPDPN) (44). The structure of 237Ab co-crystallized with a synthesized 12-mer peptide including the epitope surrounding the Tn-glycosylated Thr^{77} of mPDPN has been resolved by *Brooks et al.* (45), as shown in **Figure 5**. The GalNAc glycosylation fits perfectly inside a hydrophobic pocket, which explains why 237Ab would not recognize normally glycosylated mPDPN – the long glycan branch would not fit inside the pocket, nor would it allow the peptide to be positioned properly inside the binding cleft. 237Ab exhibited no detectable binding to the unglycosylated mPDPN backbone, demonstrating that the glycan moiety was essential for the binding either through stabilization of the epitope in mPDPN and/or directly contributes to the binding affinity. However, the binding affinity of 237Ab to free GalNAc was too low to be detected by Biacore, revealing the essential role of both the glycan- and the peptide- moieties of Tn-mPDPN to the binding by 237Ab (45).

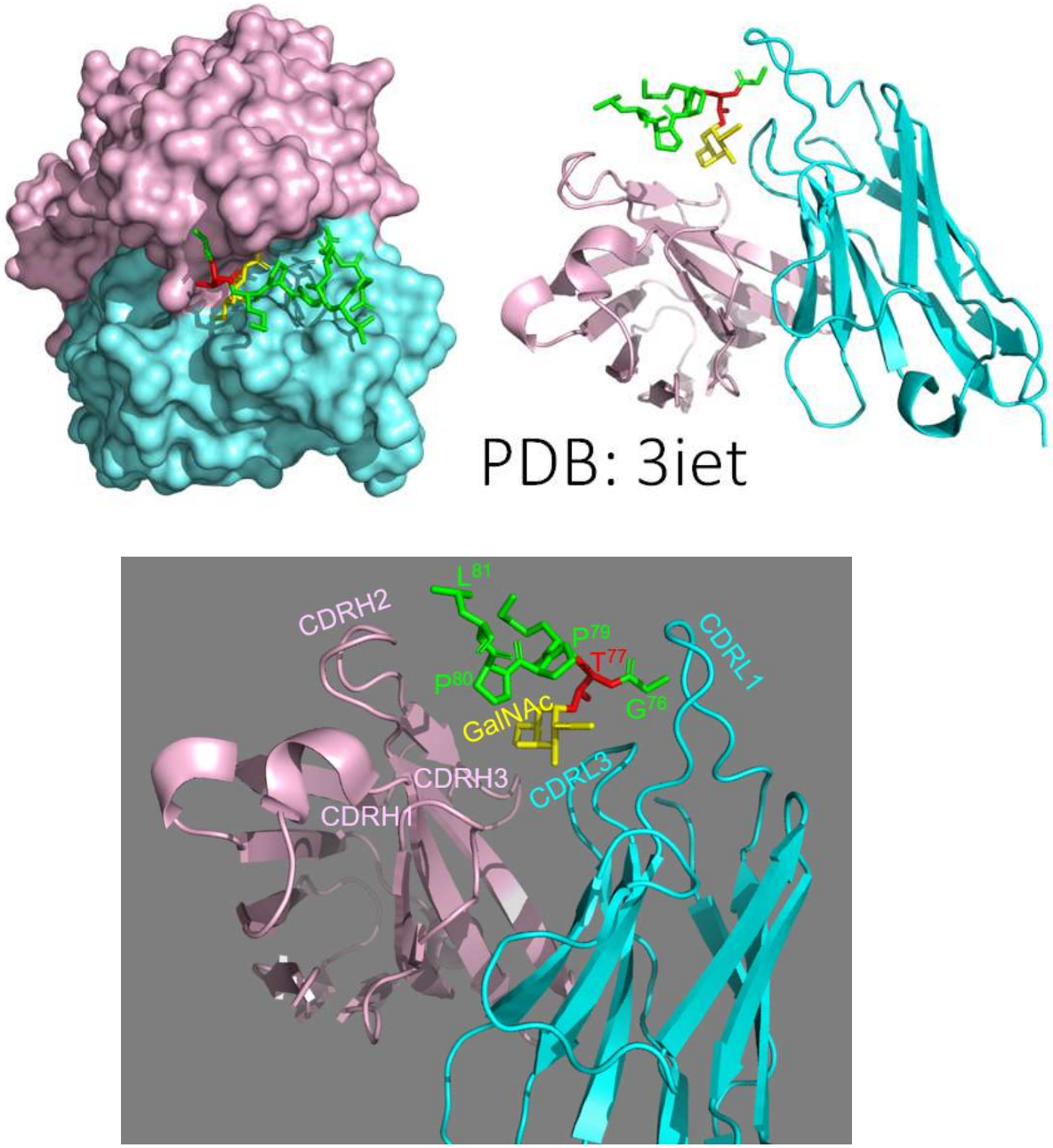

Figure 5. The structure of 237 F(ab')$_2$ co-crystallized with Tn-mPDPN fragment containing the Tn-glycosylated epitope surrounding Thr^{77} (Protein structure ID: 3iet in Protein Data Bank, PDB). Top panel: the surface (left) and the ribbon (right) diagram. Bottom panel: the ribbon and stick diagram showing the aa residues on the mPDPN backbone that are interacting with 237Ab. The figure is adopted from (45)

2. MATERIALS

2.1 Buffers and Solutions

Phosphate-buffered saline, PBS:

NaCl	0.137 M
KCl	0.0027 M
Na_2HPO_4	0.01 M
KH_2PO_4	0.0018 M

Staining buffer (for flow cytometry):

RPMI	1x
EDTA	0.005 M
BSA	1%
Sodium azide	0.02%

EAS-45 solutions

Adenine	0.02 M
Dextrose	0.11 M
Mannitol	0.055 M
NaCl	0.05 M
Glutamine	0.01 M
Na_2HPO_4	20 mM

Ammonium Chloride buffer:

NH4CL	0.155 M
KHCO3	0.01 M
EDTA	0.0001 M

Minimal imaging media (MIM):

Colorless RPMI	1x
FCS	5%
HEPES	0.01 M
probenecid	0.0025 mM

T-cell medium (TCM):

RPMI	1x
FCS	10%
Sodium Pyruvate	1x
NEAA	1x
2-mercaptoethanol	50 μM
Pen/Strep	1x

Phosphate buffer (pH 6.76) for calcium precipitation:

NaCl	1.6 g
KCl	0.074 g
Na_2HPO_4	0.05 g
HEPES	1 g
ddH_2O	Add to 100 ml

Calcium chloride buffer (2.5 M):

$CaCl_2$	36.75 g
ddH_2O	Add to 100 ml

Annealing and phosphorylation buffer:

Oligo 1 (100 mM)	1 µl
Oligo 2 (100 mM)	1 µl
10X T4 Ligation Buffer (NEB)	1 µl
T4 PNK (NEB)	0.5 µl
ddH_2O	Add to 10 µl

2.2 Kits

Name	Company	Catalog
Plasmid maxi-prep	Qiagen	12165
Mouse IFN-γ ELISA kit	Invitrogen	50-173-21
Quantibrite™ PE	BD	340495
AcGFP Calibration beads	TaKaRa	632594
MACS for mCD8+ T-cell isolation	Miltenyi	130104075
NucleoSpin® Gel and PCR Clean-up kit	Macherey-Nagel	740609

2.3 Plasmids

2.3.1 Plasmids from commercial resources

Plasmid name	Source	Cat#
pSpCas9(BB)-2A-GFP (PX458)	Addgene	48138
psPAX2	Addgene	12260
pMD2.G	Addgene	12259

2.3.2 Plasmids not available commercially but are from previous publications

Plasmid name	Source
pMFG-PDPN-IRES-EGFP	Hans Schreiber lab (44)
pMFG-COSMC-IRES-EGFP	Hans Schreiber lab (44)
pMP71-479H60	Hans Schreiber lab (46)
pMP71-1D9	Hans Schreiber lab (7)
pGEM-CD19-41BB-3z	Carl June lab (47)
pTRE-CBGluc-T2A-EGFP	Carl June lab (47)
pTRE-COSMC-P2A-CD19	Carl June lab (47)

2.3.3 Plasmids constructed for this work

Plasmid name	Source
pMP71-237-41BB-3z-EGFP	Hans Schreiber lab *
pMP71-237-41BB-3z	Hans Schreiber lab **
pMP71-5E5-41BB-3z	Hans Schreiber lab **
pMT-3H4*scF*	Hans Schreiber lab **
pMP71- CD19-41BB-3z	Hans Schreiber lab *
pMT-3H4*scFv*	Hans Schreiber lab **
pMP71-3H4-41BB-3z	Hans Schreiber lab *
pX458-COSMCKO	Hans Schreiber lab ***
pX458-MUC1KO	Hans Schreiber lab *

*constructed by Yanran He
**constructed by Boris Engels
***constructed by Steven Wolf

2.4 Primers and Oligos (all displayed in “5’-3’)

OT-I screening primers:

Transgene Forward	CTC TGC TAT GTA CTT CTG TGC C
Transgene Reverse	TTA CCT AAA ACC GTG AGC CTG

pMP71 sequencing primers:

Forward	CCCTCTCTCCAAGCTCACTT
Reverse	CAAATATGGGAATAAATGGCGGTAAGATGC

pMFG sequencing primers:

Forward	GTA GAC GGC ATC GCA GC
Reverse	GGA CTA ATC CGG ATC CTA GAG TC

pX458 sequencing primers:

Forward	ACC GAA CTG AGA TAC CTA CAG CG
Reverse	ATG TAC TGC CAA GTA GGA AAG TCC C

Guiding sequences for CRISPR-Cas9 knockout

hCOSMC	TCA CTA TGC TAG GAC AC
hMUC1	TGA AGC TGG TTC CGT GGC CG
mPDPN	GAT ATT GTG ACC CCA GGT AC

2.5 Antibodies

Table 1. Antibodies and applications

Antibody	Source	Clone	Catalog	Use	Dilution(s)
237	in-house	237	N/A	FC	1:200,*
237*scFv* tetramer	D. Kranz	237	N/A	FC	1:200**
5E5	in-house	5E5	N/A	FC	1:200,*
5F4	H. Clausen	5F4	N/A	FC	1:100,*
5E10	H. Clausen	5E10	N/A	FC	1:100
PA2.2	M. Quintanilla	PA2.2	N/A	FC	1:100
APC F(ab')$_2$ Anti-mouse IgG(H+L)	Southern Biotech	Polyclonal	1080-11L	FC	1:200
Alexa647 F(ab')$_2$ anti-mouse IgG(H+L)	Invitrogen	Polyclonal	A21237	FC	1:100
FITC g-anti-m Antibody anti-CD8a	BioLegend	53-6.7	100706	FC	1:400
FITC anti-mouse Antibody anti-CD3	BioLegend	17A2	100204	FC	1:400
PE anti-mouse Vα2 Antibody	BioLegend	B20-1	127822	FC	1:400
APC anti-mouse B220	BioLegend	RA3-6B2	103212	FC	1:400
PerCP/Cy5.5 anti-mouse-CD8a	BioLegend	53-6.7	100734	FC	1:400
αCD28 Ab	BioLegend	37.51	102116	Costim	1.5µg/ml
αCD3	UofC mAb facility	145-2C11	N/A	Costim	0.5µg/ml

* for staining with a serial dilution of Abs, starting at 3µM

** for staining with a serial dilution of Abs, starting at 30nM

2.6 Peptides

Table 2. Peptides synthesized by ELIM Biopharm

Protein Name	Abbreviation	Full sequence (* stands for GalNac)
Podoplanin (No Tn)	PDPN (no Tn)	Biotin-APLVPTQRERGTKPPLEE
PDPN-variant 9 (no Tn)	PDPN-V-9 (no Tn)	Biotin-APLVPTQRERGTKAAAA
Podoplanin	PDPN	Biotin-APLVPTQRERG(T*)KPPLEE
PDPN-variant 1	PDPN-V-1	Biotin-APLVPTQRERA(T*)KPPLEE
PDPN-variant 2	PDPN-V-2	Biotin-APLVPTQRERG(T*)APPLEE
PDPN-variant 3	PDPN-V-3	Biotin-APLVPTQRERG(T*)KAPLEE
PDPN-variant 4	PDPN-V-4	Biotin-APLVPTQRERG(T*)KPALEE
PDPN-variant 5	PDPN-V-5	Biotin-APLVPTQRERG(T*)KPPAEE
PDPN-variant 6	PDPN-V-6	Biotin-APLVPTQRERG(T*)KPPLAE
PDPN-variant 7	PDPN-V-7	Biotin-APLVPTQRERG(T*)KPPLA
PDPN-variant 8	PDPN-V-8	Biotin-APLVPTQRERG(T*)KPAAA
PDPN-variant 9	PDPN-V-9	Biotin-APLVPTQRERG(T*)KAAAA
PDPN-variant 10	PDPN-V-10	Biotin-APLVPTQRERG(T*)AAAAA
PDPN-variant 11	PDPN-V-11	Biotin-APLVPTQRERA(T*)AAAAA
PDPN-variant 12	PDPN-V-12	Biotin-APLVPTQRERG(T*)KAAA
PDPN-variant 13	PDPN-V-13	Biotin-APLVPTQRERG(T*)KAA
PDPN-variant 14	PDPN-V-14	Biotin-APLVPTQRERG(T*)KA
PDPN-variant 15	PDPN-V-15	Biotin-APLVPTQRERG(T*)K

Table 3. Peptides synthesized by Synpeptide		
Protein Name	Abbreviation	Full sequence (* stands for GalNAc)
Transferrin receptor protein 1	TFRC	Biotin-EPKTECERLAG(T*)ESPVRE
Mucin 1	MUC1	Biotin-SAPDTRPAPGS(T*)APPAHG
Zinc transporter ZIP6	ZIP6	Biotin-GKLFPKDVSSS(T*)PPSVTS
Podocalyxin-like protein 2	PDXL	Biotin-SSHSVTTDLTS(T*)KAEHLT
Leukosialin	CD43	Biotin-PPLTMATVSLE(T*)SKGTSG
Protein EVI2B	EVI2B	Biotin-SRKQITVHNPS(T*)QPTSTV
Protocadherin-9	PCDH	Biotin-LNISHINAATG(T*)SASLVY
Lysosome-associated membrane glycoprotein 1	LAMP	Biotin-TRCEQDRPSPT(T*)APPAPP

2.7 Cell lines

2.7.1 Parental cell lines (including variants received from other research groups)

Murine cell lines:

- Ag104A (in house) (43)
- Ag104A-PDPN$^{-/-}$

The mPDPN-negative variant was made by CRISPR-Cas9 mediated knockout of mPDPN using the following guiding sequence: GAT ATT GTG ACC CCA GGT AC. The cell line was received from H. Clausen's lab.

- Neuro2A was from G. Ragupathi and P.O. Livingston (48)

Human cell lines:

- Jurkat E6-1, a gift from C. June at the University of Pennsylvania (47)
- Jurkat E6-1 CBGluc-T2A-EGFP, a gift from C. June at UPenn (47)
- Jurkat E6-1 CBGluc-T2A-EGFP, COSMCWT-P2A-CD19, received from C. June at UPenn (47)
- SKOV3, a gift from E. Lengyel at the University of Chicago
- T47D (ATCC®HTB-133™)

2.7.2 Cell line variants established during this work

Murine cell lines:

- Ag104A-COSMC-wildtype
- Ag104A-mPDPN$^{-/-}$-COSMC-wildtype

The COSMC-wildtype variant was generated by retroviral transduction of pMFG-COSMC-IRES-EGFP encoding the wildtype murine COSMC.

- Neuro2A-PDPN
- Neuro2A-COSMC-wildtype

The mPDPN-positive variant was made by transduction of the retroviral vector pMFG-PDPN-IRES-EGFP encoding mPDPN as described (44). The COSMC wildtype variant was made by transduction of the cell line with retroviral vector pMFG-COSMCWT-IRES-EGFP encoding the wildtype murine COSMC.

Human cell lines:

- Jurkat E6-1 CBGluc-T2A-EGFP-PDPN:

The mPDPN-positive variant of Jurkat E6-1 CBGluc-T2A-EGFP was made by transduction of the cell line with retroviral vector pMFG-PDPN-IRES-EGFP (44)

- Jurkat E6-1 CBGluc-T2A-EGFP, COSMC-P2A-thCD19-PDPN

The mPDPN-positive variant of Jurkat E6-1 CBGluc-T2A-EGFP, COSMC-P2A-thCD19 was made by retroviral transduction of pMFG-PDPN-IRES-EGFP encoding the wildtype murine PDPN as described (44).

- Jurkat E6-1 MUC1$^{-/-}$

The *MUC1* knockout variant was prepared by CRISPR-Cas9 knockout using the following guiding sequence: TGA AGC TGG TTC CGT GGC CG.

– SKOV3-COSMC $^{-/-}$*

The *COSMC* knockout variant was made by CRISPR-Cas9 knockout using the following guiding sequence: TCA CTA TGC TAG GAC AC.

– SKOV3-mPDPN

The mPDPN-positive variant was made by transduction of the retroviral vector pMFG-PDPN-IRES-EGFP encoding the wildtype mPDPN as described (44).

– T47D- *COSMC* $^{-/-}$

The *COSMC* $^{-/-}$ variant was made by CRISPR-Cas9 knockout using the following guiding sequence: TCA CTA TGC TAG GAC AC.

All cell lines but the Jurkat parental and its variants were maintained in DMEM medium supplemented with 10% FCS, 100 U/ml penicillin-streptomycin, cultured at 37°C and 10% CO_2 in a dry chamber. Jurkat and its variants were maintained in RPMI 1640 medium supplemented with 10% FCS, 100 U/ml penicillin-streptomycin, incubated at 37°C and 5% CO_2 in a dry chamber.

*A cell line made by Steven Wolf

2.8 Mice

2.8.1 Mice from commercial resources

- B6.129S7-Rag1^{tm1Mom}/J, also known as B6-Rag1$^{-/-}$, is bought from Jackson Laboratory (Bar Harbor, ME)
- C57BL/6-Tg (TcraTcrb)1100Mjb/J, also known as OT-I; is bought from Jackson Laboratory (Bar Harbor, ME)
- NOD.Cg-Prkdcscid Il2rgtm1Wjl/SzJ, also known as NSG, is bought from Jackson Laboratory (Bar Harbor, ME).
- C3H Rag2$^{-/-}$ mice were purchased from Taconic.
- C3H CD8$^{-/-}$ mice were the >20 generations backcrossing of B6CD8$^{-/-}$ (B6.129S2-Cd8atm1Mak/J, Jackson Laboratory (Bar Harbor, ME)) to C3H/HeN (NIH)

2.8.2 New mice strain bred in-house for this work

- The B6-Rag1$^{-/-}$ was bred to OT-I to generate OT-I x Rag1$^{-/-}$ mice. Mice were bred at The University of Chicago, Carlson Animal Research Facility

3 METHODS

3.1 Flow cytometry

To determine Ab binding to different cancer cell lines, $1x10^5$ cells of each cancer type were incubated with primary Ab at indicated concentrations in staining buffer (SB, See Buffers and Solutions) for 20 min at 4°C, then washed in SB twice, and incubated with secondary APC-goat anti-mouse IgG(H+L) polyclonal Ab (Southern Biotech) in SB for 20 min at 4°C. Cells were analyzed by flow cytometry (LSR II, BD Bioscience) after additional washing in SB. Data were analyzed using the Flowjo software (TreeStar). The level of primary Ab binding was determined by the binding ratio, which represents the value of median fluorescence intensity (MFI) of cells stained with primary and secondary Abs divided by the MFI of the corresponding cell line stained with the secondary Ab only.

3.2 Immobilization of biotinylated peptides on streptavidin coated plate

To immobilize biotinylated peptides to plate surface, 50 µl 10 µg/ml streptavidin in double distilled water was left dried on each well of an immunosorbent plate (Nunc) at room temperature overnight. The unbound surface of the plate was blocked by 50 µl assay diluent (eBioscience) at room temperature for 1 h. After washing 3 times by PBST (PBS, 0.5% Tween 20), biotinylated peptides diluted in 50 µl assay diluent were added to the plate in indicated concentrations, incubated at room temperature for 2 h before testing for antibody binding or activation of CART.

3.3 Loading of biotinylated peptides on streptavidin coated RBC

RBCs were isolated from whole blood and were biotinylated using different concentrations of biotin-X-NHS according to manufacturer's instructions. The cell surface biotinylation was detected by PE-streptavidin conjugate (eBioscience), and the density of

surface biotinylation was quantified by using BD Quantibrite™ PE fluorescence Quantification Kit. To load biotinylated Tn-glycopeptides onto the surface of RBCs, the RBCs were first incubated with 1mg/ml streptavidin (Sigma) at 4 °C for 30min, washed twice with EAS-45, and then the biotinylated Tn-glycopeptides were added onto the streptavidin coated-RBC at a saturating concentration of 20 μg/ml for 2D affinity measurements as described (49).

3.4 Detection of Ab binding to the peptides immobilized on the plate surface

50 μl 10 μg/ml 237Ab or 5E5Ab in 1x assay diluent (Invitrogen) was added to each well containing immobilized peptides and incubated for 1 h at room temperature. After washing three times with PBST, goat-anti-mouse IgG-HRP (Invitrogen) was added to each well and incubated for 30 min at room temperature. After washing 5 times with PBST, 50 μl 5,5'-tetramethylbenzidine TMB (eBioscience) was added to each well and 25 μl 2 N sulfuric acid was added to stop the reaction. The level of Ab binding was determined by light absorption at 450 nm, read by the microplate reader VERSAmax (Molecular Devices).

3.5 T-cell transduction

Retroviral supernatant used for T-cell transduction was produced by transiently transfecting Plat-E packaging cells with pMP71-237CAR/5E5CAR/CD19CAR by calcium phosphate precipitation as previously described (6). Virus supernatant harvested 48 and 72 h post transfection was used for transduction of splenocytes isolated from OTI-Rag1$^{-/-}$ mice after 24 h pre-stimulation by plate-coated αCD3 (Clone 145-2C11, University of Chicago Frank W. Fitch monoclonal antibody facility) and αCD28 Ab (Clone 37.51, Biolegend) in the presence of 40 U rhIL-2 (Peprotech). The stimulated cells were spinoculated in plates pre-coated with RetroNectin (12.5 μg/mL in PBS, overnight at 4°C, TaKaRa, Otsu, Japan) together with virus supernatant in presence of 4 μg/ml protamine sulfate (Sigma Aldrich) at

800 g, 32 °C for 90 min. The transduced T cells were maintained in the T-cell medium (TCM, RPMI 1640 (Invitrogen), 10% heat-inactivated FCS (Sigma), 1 mM sodium pyruvate, 1 mM HEPES, 100 IU/ml penicillin, streptomycin (all: Invitrogen), 50 μM 2-mercaptoethanol (Sigma Aldrich, prepare 50 mM pre-dilution in RPMI 1640 and add always fresh) containing 50 ng/ml recombinant human IL-15 (Peprotech) for additional 5 days or frozen in the liquid nitrogen for long-term storage.

3.6 Ca^{2+} influx assay

For Ca^{2+} flux experiments, 10^6 237CART cells were incubated with 5 μM of fluorescent dye Fluo-4 AM (Molecular Probe) for 30 min in complete RPMI-1640, 2.5 mM probenecid. 10 min before data collection, the T cells will be washed twice with MIM and resuspended in 200 μl MIM (50). For calcium influx imaging, a LEITZ DMIRB Leica Microscope equipped with a 100× objective was used, and the data was acquired by an iXON Ultra 888 EMCCD Camera. The Fluo-4 stained T cells co-incubated with each different type of cancer stimulators were illuminated sequentially by blue light (470 ± 20 nm) and white light at 100ms interval for up to 20 min, the light trigger, and data acquisition were controlled by μManager (51). The data were processed and analyzed by Fiji software.

3.7 2D micropipette kinetic assay

For 2D measurement of CAR binding to the ligands between a CAR T-cell and a ligand-loaded RBC, 237CARGFP-transduced T cells were used with the number of CAR molecules per T cells quantified by AcGFP Flow Cytometer Calibration Beads (TaKaRa) according to the manufacturer's protocol. The micropipette experiments were performed as described (52) with the ligand-loaded RBC repeatedly driven to get in touch with 237CART for a controlled duration of contact time (0.25, 0.5, 0.75, 1, 2, and 5 s). Adhesion events are defined by

elongation of RBC during cell separation and were recorded manually by observations during the 50 repeated contact-retract cycles. Unglycosylated PDPN was used for subtracting the non-specific binding:

$$P_a = \frac{(P_{measured} - P_{nonspecific})}{1 - P_{nonspecific}} \quad (1)$$

The probability of adhesion at each different contact time can be fitted into the following probabilistic model (53):

$$P_a = 1 - exp\{-m_r m_l A_c K_a [1 - exp\ (-k_r t)]\} \quad (2)$$

Where m_r and m_l are the respective CAR and peptide ligand densities that were measured by flow cytometry. A_c is the contact area between the two cells. The fitted curve by GraphPad shall generates effective 2D affinity $A_c K_a$ and off-rate k_r, and the $A_c k_{on}$ can be calculated by

$$A_c k_{on} = A_c K_a \times k_r \quad (3)$$

3.8 Cytokine release assay

Cytokine release assay of effector CART in recognition of stimulator T cells.

10^4 CAR-modified OTIxRag1$^{-/-}$ T cells were co-cultured with target cells at the indicated stimulator-to-responder ratio or with immobilized peptides coated at the indicated coating concentration for 24 h. The level of IFN-γ release into the medium was measured by ELISA (Invitrogen).

*Cytokine release assay of effector CART in recognition of immobilized peptides on the plate surface***.**

After the peptides had been immobilized on the plate surface, the wells were washed with PBST once and with RPMI for additional 3 times. 10^4 CAR-expressing T cells were added to each well of the 96-well plate. After 24 h of coincubation with the immobilized peptides in TCM, the level of IFN-γ release in the medium was determined by ELISA (Invitrogen).

3.9 ^{51}Cr release assay

The capability of CAR-engineered T cells to lyse target cells was evaluated in a 4 h ^{51}Cr release assay. Target cells were incubated with 25 μCi sodium chromate-51 (Perkin Elmer) in the culture medium for 1 h, washed 3 times with the culture medium, and resuspended at $1x10^5$ cell/ml. 50 μl target cell suspension (n = 5,000) was mixed with 50μl effector CART suspension in each well of a U-bottomed 96-well cell culture plate (Fisher) at the indicated effector-to-target ratios. The positive control was set using ZAP-OGLOBIN II lytic reagent according to the manufacturer's instruction (Beckman Coulter 7546138). Target cells cultured in the culture medium alone were used as spontaneous control. After 4 h of co-incubation, 50μl supernatant from each well was collected and transferred into scintillation tubes. Target killing was evaluated by the level of radioactivity released into the medium measured by an automatic γ counter (Titertek). The percentage of target lysis was calculated by the following formula: (experiment-spontaneous)/(maximum-spontaneous) x100.

3.10 Epifluorescence microscope

For killing assay monitored by epifluorescence imaging. 70,000 GFP-positive Jurkat, Jurkat-PDPN or Jurkat COSMC-wildtype cells were immobilized on plate surface using anti-human CD45 Ab in each well of the 8-well LabTek Chamber Slides (Nalge Nunc, Naperville, IL). 70,000 sorted 237CARGFP-transduced OTIxRag1$^{-/-}$ were added to each well and data was acquired using a Zeiss Axioplan microscope (Zeiss. Thomwood, NY) and a Photometries

PXL CCD camera (Biomedical Photometries) at 10 s interval at 11/10/13 different positions respectively for Jurkat, Jurkat-PDPN or Jurkat COSMC-wildtype using the following parameters:

Frames	600
Exposure	100 ms
DIC	30 ms, 25%
LED	470 nm, 100 ms
Intensity	5%
EM Gain	300

The workflow of analyzing the data is explained as below:

1. Separate each Raw .tff file to 3 channels:
   - -DIC
   - -GFP
   - -Death Indicator (forgot its name..)

2. Use ImageJ to analyze the GFP channel:
   - -Background subtraction (Rolling Ball algorithm)
   - -Tracking of Cancer Cells
   - -Filter spots and tracks
   - -Identify centroids spots for 'alive' or 'dead'

3. Pre-process data to prepare for classification
   - -Calculate time and attach sample ID
   - -Sort into different tracks
   - -Calculate %change in r and intensity for each track
   - -Extract other useful features e.g. SNR, contrast etc.
   - -Build up a feature table for classification

4. Classification of Spots into 'alive' or 'Dead'
   - -Calculate time and attach sample ID
   - -Sort into different tracks
   - -Calculate %change in r and intensity for each track
   - -Extract other useful features e.g. SNR, contrast etc.
   - -Build up a feature table containing all spots
   - -Use K-mean clustering to classify, using above identified centroids

5. Post-process data and plot
   - -Resort spots into different tracks and timepoints
   - -Calculate %killing at each timepoints for each sample
   - -Average over samples in each group and plot

*

*The procedure is generated by Guoshuai Cao from Jun Huang's lab

3.11 Leukemia/tumor transplantation

– NSG mice were selected as the recipients for Jurkat leukemia. $5x10^6$ cancer cells were transplanted through tail-vein injection
– B6Rag1$^{-/-}$ mice were selected as the recipient for SKOV3 and Ag104A. $5x10^6$ SKOV3 or $5x10^5$ Ag104A cells were s.c. transplanted. Treatment or control treatment was given around 14-21 days after tumor transplant depending on the tumor growth (~500 mm^3)
– C3HRag2$^{-/-}$ mice were selected as the recipients for Ag104A and Ag104A-mRLRP9. $5x10^5$ cancer cells were transplanted subcutaneously and the animals were treated around 7 or 14 days after tumor transplantion with the combination of 237CAR-OT1Rag1$^{-/-}$ and 479H60-C3HCD8$^{-/-}$ T cells.

3.12 Live animal imaging

Jurkat cells were modified to express Click Beetle Green (33). $5x10^6$ Jurkat cells were injected through tail vein and disease progression was monitored weekly by bioluminescence imaging on a Xenogen IVIS-200 Spectrum camera (Perkin Elmer). D-luciferin, potassium salt (Goldbio) was injected i.p. according to manufacturer instruction 15 min before imaging.

3.13 Tumor digestion for separation of TILs using MACS

An appropriate piece of the tumor (~100 mm^3 pinky, live tissue) was placed in a 35 x 10 mm dish, chopped into smaller pieces, and then the tissue was ground thoroughly with a cell strainer and the back of a 1ml syringe. Then the sample was transferred into a 15 ml conical bottom tube, washed once with 10 ml plain RPMI, and then resuspended in 5 ml RPMI, 10% FBS. Collagenase D (Roche) and DNase I (Roche) were added to the ground tumor tissue at 2 mg/ml and 100 U/ml respectively, incubated with the sample on a benchtop shaker at RT for 1h. 600 µl 10 x Trypsin (Sigma-Aldrich) was subsequently added to the sample, and

incubated with the sample on the benchtop shaker for additional 30 min. Then the sample got washed once with 15 ml RPMI, filtered through a 70 µm- and 45 µm- cell strainer. Counted the harvest, concentrated it to a desired concentration by centrifugation at 350 g, 10 min. The sample was then ready to be used for MACS for separation of CD8a+ TILs

3.14 CRISPR knockout

To clone the guiding sequence into the sgRNA scaffold, a pair of standard de-salted oligos covering the guiding sequence were ordered from Integrated DNA Technologies, Inc. (IDT). The guiding sequence was proceeded by 5'-CACCG-3', and its reverse complement sequence was proceeded by 5'-AAAC-3', followed by an 'C' in the '-3' end as demonstrated below:

5' – CACCGNNNNNNNNNNNNNNNNN – 3'

3' – CNNNNNNNNNNNNNNNNNNCAAA – 5'

The oligos were reconstituted in double distilled water to 100mM, and then diluted to 10mM in the phosphorylation and annealing buffer as described in the Materials-solutions (page 26). The pair of oligos were then phosphorylated and annealed in a thermocycler (T100^{TM} of BIO-RAD) by running the following program:

37 ^{o}C	30 min
95 ^{o}C	5min and then ramp down to 25 ^{o}C at 5 ^{o}C/min

The *Bbs*I (NEB) digested plasmid pX458 for accepting the phosphorylated and annealed oligos was prepared as described below:

pX458	1 µg
1X NEB Buffer™ 2.1	1 µl
BbsI	0.5 µl
ddH2O	Add to 10 µl total

The above mixture was incubated at 37 ºC for 1 h, then the calf intestinal alkaline phosphatase, CIP (NEB) was added and the mixture was incubated at 37 ºC for an additional hour for dephosphorylation. The digested and dephosphorylated plasmid was then purified by using NucleoSpin® Gel and PCR Clean-up kit (Macherey-Nagel).

The dephosphorylated and digested plasmid with the phosphorylated oligos were then annealed together as below:

Digested and dephosphorylated pX458	50 µg
Phosphorylated and annealed oligos (1:200)	1 µl
10 x T4 ligase buffer (NEB)	2 µl
ddH2O	Add ddH_2O to 20 µl total

The mixture was incubated at room temperature for overnight. Afterwards the competent bacteria (TOPO10, Invitrogen) was transfected with 5 µl of the ligation product.

3.15 Statistical analysis.

Data were analyzed using Prism software (GraphPad). Error bars in the figures indicate SEM of at least 2 independent experiments. For the comparison of two groups where the data was normally distributed, the Student's t-test (two-tailed) was used. For comparison of data that are non-parametric, Wilcoxon Rank Sum Test was employed. The significance level of the difference between the survival of animals from the different treatment groups was determined by the log-rank Mantel-Cox test. For comparison of multiple groups, one-way ANOVA corrected with Tukey's multiple comparisons was employed when appropriate. In the figure legend, ns stands for $p > 0.05$, * stands for $p \leq 0.05$, ** stands for $p \leq 0.01$, *** stands for $p \leq 0.001$, **** stands for $p \leq 0.0001$.

4 RESULTS

4.1 237CART recognizes COSMC-mutant cancer cells not predicted by 237Ab staining

– Introduction

Previous work has demonstrated the exceptional cancer-specificity of 237Ab for a Tn-glycosylated epitope in murine podoplanin (mPDPN) that result from COSMC mutation. I intended to combine the cancer-specificity of 237Ab and the potency of therapeutic T cells, by constructing a CAR that conducts potent T-cell killing guided by 237Ab specificity. To this end, the single-chain variable fragment (*scFv*) of 237Ab was fused to the intracellular signaling component of 4-1BB, a TCR co-stimulatory signal, and the intracellular signaling domain of CD3ζ, to make a second-generation CAR construct (10). In this chapter, I generated 237CAR-transduced primary T cells, and determined the activity and specificity of CART cells *in vitro*, in comparison to that of the original 237Ab. In order to better understand the *scFv* used in the 237CAR construct and to determine the significance of avidity may have on target recognition, the staining of COSMC-mutant or wildtype cell lines with or without mPDPN expression by 237*scFv* tetramers was also compared to staining by 237Ab.

– Results

237CAR expression on transduced primary T cells can be detected by staining with polyclonal fluorophore-labeled F(ab')$_2$ anti-mouse IgG(H+L)

237CAR construct was made by fusing the nucleotide sequence coding for a single chain variable fragment (*scFv*) of 237Ab with a murine CD28α hinge and CD28 transmembrane domain, a 4-1BB co-stimulatory domain and a CD3ζ activation domain in a linear fashion, modeled off a publication by Zhang and Harris as described previously (54). The CAR construct* was ordered from GeneArt and was inserted into the retroviral vector MP71 as described before (55). 237CART was prepared by retrovirally transducing OTIRag1$^{-/-}$ splenocytes with the construct (7). CAR expression on the T-cell surface was detected by Alexa647 F(ab')$_2$ anti-mouse IgG(H+L) staining at the indicated dilutions. As it has been shown in (**Figure 6**). The CAR-transduced T cells were specifically stained at all staining concentrations but worked the best at 1:250 dilution. Therefore, 1:250 dilution was used for detecting CAR expression in the rest of the study.

*The 237CAR construct was designed and ordered by Dr. Boris Engels

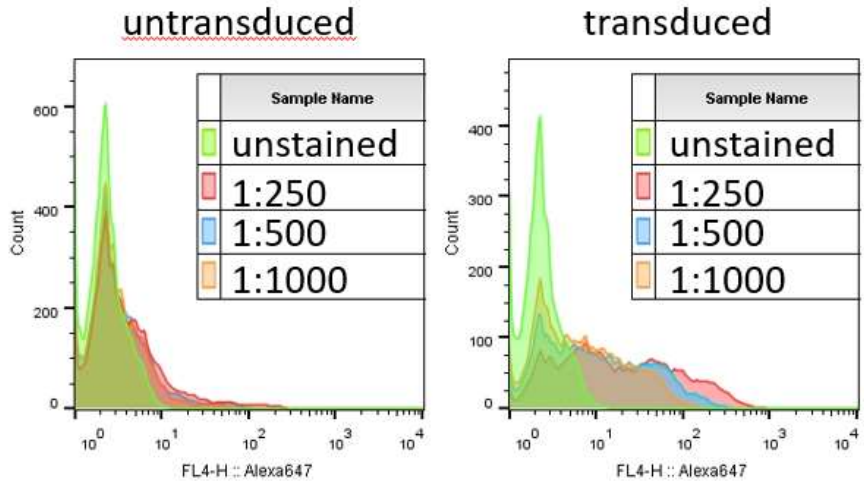

Figure 6. Detection of CAR expression on transduced primary T cells using F(ab')$_2$ anti-mouse IgG(H+L) to recognize the *scFv* of 237CAR on the cell surface. Alexa647-coupled F(ab')$_2$ anti-mouse IgG(H+L) were used at the indicated dilutions of the stock to stain either the 237CAR-transduced or the mock-transduced cells. Data were acquired on an LSR-II (BD). The Ab binding level was determined by the median fluorescence intensity (MFI).

237CART recognizes COSMC-mutant cancers not predicted by 237Ab

The general notion when constructing a CAR from an Ab is that the CAR will follow the specificity of the Ab. To compare the specificity of 237Ab and 237CART, cancer cells of 3 distinct cellular backgrounds were used to determine the binding by 237Ab and recognition by 237CART.

Ag104A, a murine sarcoma naturally expresses mPDPN and carries a COSMC mutation that causes a 26 aa deletion in the C-terminal region that completely disrupts normal COSMC function. Ag104A is positive for 237Ab staining (**Figure 7**). However, when the mPDPN is knocked out from Ag104A cells by CRISPR-Cas9 targeting the exon 1 of *Pdpn* using the guiding sequence GAT ATT GTG ACC CCA GGT AC, the cell line becomes negative for 237Ab staining even at a supraphysiological high concentration (~3000nM). Nevertheless, 237CART can be activated by Ag104A-PDPN$^{-/-}$ and lysed Ag104A in the presence or absence of mPDPN but invariantly dependent on COSMC mutation (**Figure 8**). Similar patterns of recognition by 237CART were also observed in the cells from Jurkat human leukemia or SKOV3 human ovarian cancer background. mPDPN is naturally not present in either one of the human cancer cell lines, the ectopic mPDPN expression was introduced by retroviral transduction of *Pdpn*. Jurkat naturally carries a premature stop mutation in COSMC, and the COSMC-wildtype counterpart was created by lentiviral transduction of the wildtype human COSMC gene. While SKOV3 naturally has normal COSMC function, the gene was knocked out by CRISPR-Cas9 using the guiding sequence TCA CTA TGC TAG GAC AC.

Altogether, COSMC-mutant cancers from 4 independent cellular backgrounds all activated 237CART to release IFN-γ and were lysed by 237CART cells independent of mPDPN expression. In all cellular backgrounds, regardless of mPDPN expression, restoration

of wildtype COSMC expression completely abolished T-cell activation, demonstrating the recognition by 237CART is dependent on the cancer-specific COSMC mutation (**Figure 8**). The 237CART recognition of mPDPN-negative COSMC mutant cancers would not have been predicted by 237Ab staining **(Figure 7)**, however expanding the application of 237CART to multiple different human cancers without recognizing normal tissues due to its dependence on the cancer-specific COSMC mutation.

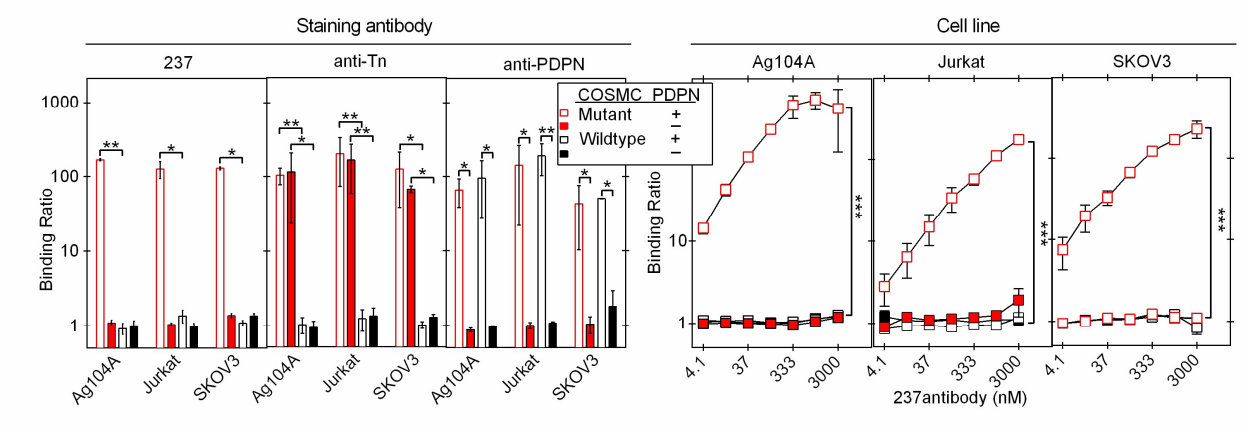

Figure 7. 237Ab specifically stains COSMC-mutant cancers with mPDPN expression. The COSMC-mutant or -wildtype variants of each cell line with or without mPDPN expression from 3 distinct cellular backgrounds: Ag104A (COSMC-mutant, mPDPN positive) , Jurkat (COSMC-mutant, no mPDPN expression) and SKOV3 (COSMC wildtype, no mPDPN expression) , were generated using CRISPR/Cas9 knockout (COSMC-mutant variants of SKOV3 and mPDPN negative variants of Ag104A) and viral transduction (COSMC-wildtype variants of Ag104A and Jurkat; and mPDPN expressing variants of Jurkat and SKOV3). **Left**, each cell line was stained with either 237, anti-Tn Ab 5F4, or anti-mPDPN Ab PA2.2 at the concentration as indicated in Table 1. **Right,** each cell line was stained with a serial 3-fold dilution of 237Ab, started at 3μM. The binding of primary Abs was detected by $F(ab')_2$ anti-mouse IgG(H+L) coupled with APC, used at a 1:200 dilution. The binding levels of primary Abs were compared by the "binding ratio", the MFI of primary and secondary Abs double staining divided by the MFI of staining with secondary Ab only. The statistical significance of the differences between two groups as pointed by the bracket was calculated by Student's t-test. Mean ± SEM, n = 3.

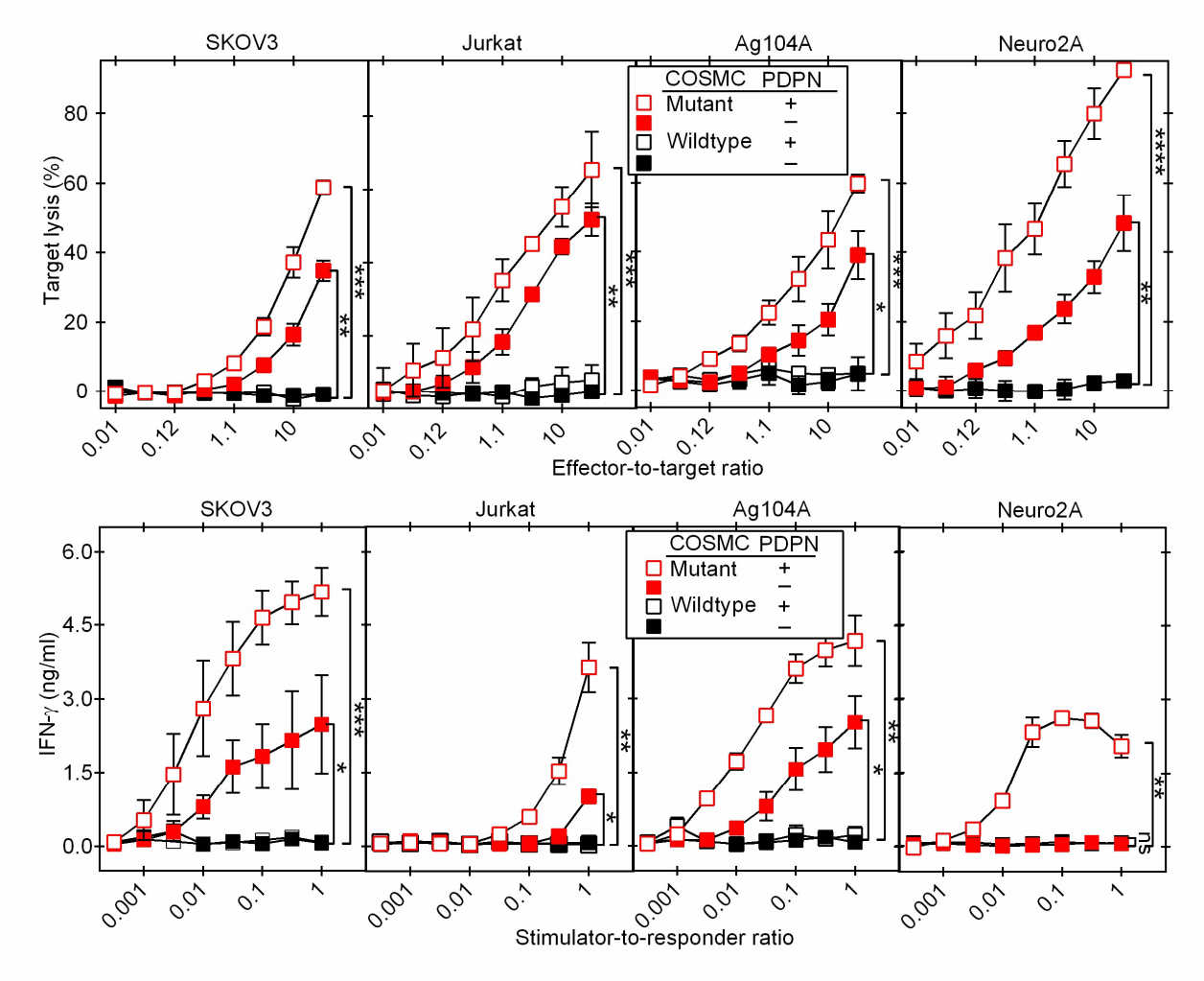

Figure 8. 237CART recognition of COSMC-mutant or wildtype cell lines with or without mPDPN expression. **Top panel**: The activation of 237CART was determined by the percentage of target lysis by 237CART in a classical 4-hr ^{51}Cr release assay, 5,000 targets per well, incubated with effector 237CART at the effector-to-target ratio as indicated in the figure. **Bottom panel:** The activation of 237CART was determined by the level of IFN-γ release into the medium from 10,000 237CART cells as responders incubated with stimulator cells at the stimulator-to-responder ratio as indicated for 24 h. The significance of the difference between two groups as pointed by the bracket was examined by Student's t-test. Mean ± SEM, n = 3.

Tn-mPDPN stimulated stronger and more durable T-cell activation compared to Tn-glycopeptide antigens not predicted by 237Ab binding

Jurkat leukemia is naturally *COSMC*-mutant (30) and is not expressing mPDPN as a human cancer cell line. All of the *O*-linked glycosylations on the cell surface are Tn-glycosylated due to its dysfunctional *COSMC* mutation. I have examined 237CART activation upon recognition of Jurkat either with or without mPDPN expression. In a T-cell activation assay measured by calcium influx signals (56), Jurkat expressing Tn-mPDPN induced a stronger and more durable Ca2+ influx than that induced by Jurkat without Tn-mPDPN expression (Figure 9A)*. Similarly, the killing of target cells in real-time was monitored by epifluorescence microscopy** (Zeiss Axioplan microscope (Zeiss. Thomwood, NY) and recorded on a Photometries PXL CCD camera (Biomedical Photometries), using 70,000 target cells immobilized on the bottom of each well of an 8-well LabTek Chamber slide co-incubated with 70,000 237CART cells since the beginning of video acquisition. The target cell channel from the videos was extracted with the following downstream processing. The background was first removed, and then the cells were segmented and tracked with Trackmate package in Fiji software. The parameters about each cell in each frame of every video including: Mean Intensity, Median Intensity, Minimum Intensity, Maximum Intensity, Total Intensity, Standard Deviation, Estimated Diameter, Contrast, SNR (Signal to Noise Ratio) were recorded. The statistics of all cells in all frames were then pooled and normalized for comparison. A support vector machine (SVM) classifier was then built by training on the cells from the first (defined as ‘all alive’) and the last 5 (defined as ‘all dead’) frames of all videos, with 5-fold cross-validation. The classifier was then optimized using a validation set consisting of cells from frame 5-10 as “viable” and cells from the last 10-5 frames as “dead”.

Finally, the classifier was used to identify the viability of every cell in every frame, and the average percentage of cells classified as “dead” was monitored as the killing efficiency. The results have demonstrated that the presence of mPDPN significantly enhanced target killing compared to that without, and the target killing was completely abolished by ectopic expression of COSMC-wildtype (Figure 9B) **.

* Yanran He prepared the effector and target cells for the experiment, while the calcium influx experiment was performed by Dr. Wei Feng, and the data were analyzed by Guoshuai Cao from Dr. Jun Huang’s lab

** Yanran He prepared the effector and target cells for the experiment, while the target killing assay was performed and analyzed by Guoshuai Cao from Dr. Jun Huang’s lab

A.

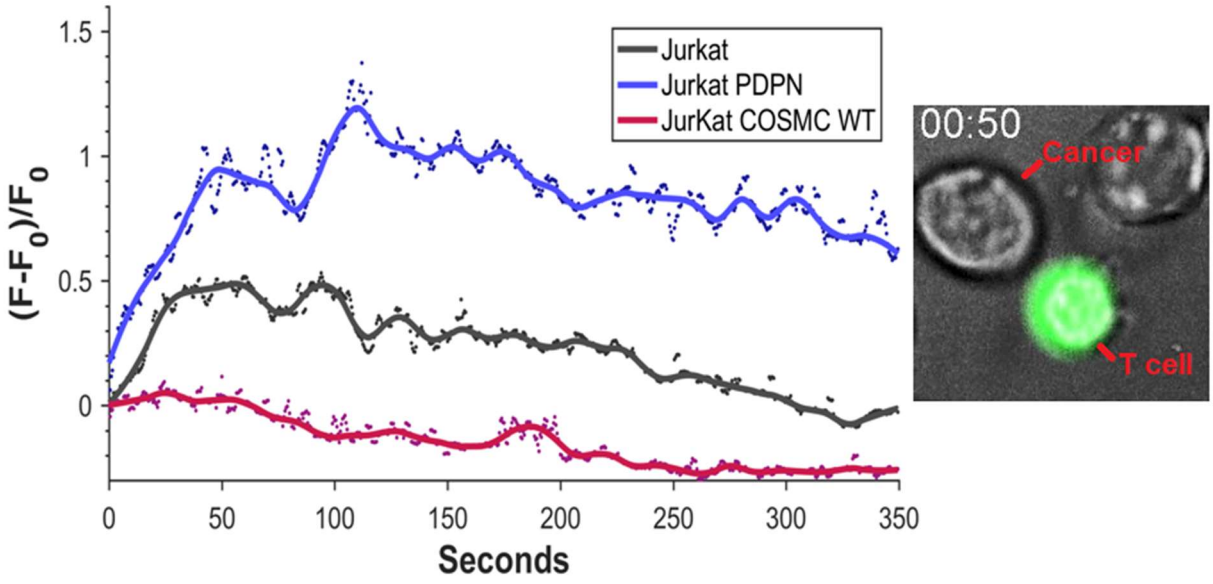

B.

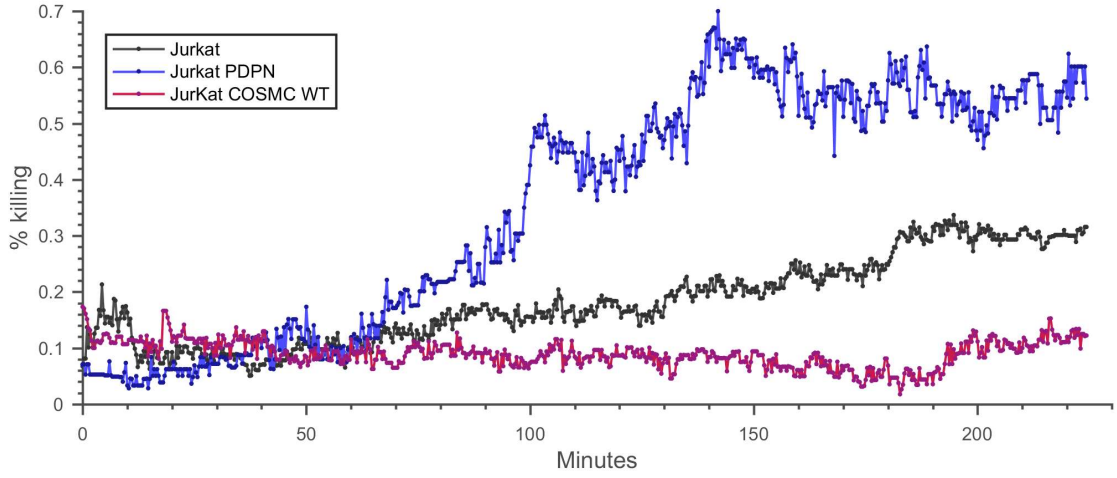

Figure 9. The activation of 237CART in recognition of cancer targets in real-time. **A.** Calcium influx assay of 237CART in recognition of Jurkat variants*. 70,000 237CART cells were labeled with fluo-4 and added to plate (8-well LabTek Chamber slides) with immobilized Jurkat (using anti-human CD45 Ab) on the surface. The data were acquired on the LEITZ DMIRB Leica Microscope equipped with a 100× objective and an iXON Ultra 888 EMCCD Camera.

Figure 9, continued. Blue light (470 ± 20 nm) and a white light were illuminated sequentially at 100ms interval for up to 20 min. The data was processed and analyzed by Fiji software. **B.** Target killing by 237CART in recognition of different Jurkat variants**. 70,000 237CART cells were incubated with 70,000 target cancer cells in each well of an 8-well LabTek Chamber slides and the target killing events were monitored by epifluorescence imaging. The data were acquired on a Zeiss Axioplan microscope (Zeiss. Thomwood, NY) and a Photometries PXL CCD camera (Biomedical Photometries). A support vector machine (SVM) was trained on cells from the first 5 frames of all videos (only 'live' events), and cells from the last frames of all videos (only 'dead' events) with 5-fold cross-validation to identify 'live' and 'dead' events. The classifier was then optimized using a validation set consisting of cells from frame 5-10 as "viable" and cells from the last 10-5 frames as "dead". Finally, the classifier was used to identify the viability of every cell in every frame, and the average percentage of cells classified as "dead" was used to determine the killing efficiency.

* Yanran He prepared the effector and target cells for the experiment, while the calcium influx imaging was performed by Dr. Wei Feng, and the data were analyzed by Guoshuai Cao from Dr. Jun Huang's lab

** Yanran He prepared the effector and target cells for the experiment, while the target killing assay acquired on an epifluorescence microscope was performed and analyzed by Guoshuai Cao from Dr. Jun Huang's lab

237CART specifically recognizes the Tn-glycopeptides but not STn-glycopeptides in COSMC-mutant cancers.

COSMC-mutant cancers could not only carry Tn but also STn antigens depending on the activity of sialyl-transferase ST6GalNAc-I that catalyzes the sialylation of Tn. (**Figure 10**). To determine whether if 237CART can be activated by STn-glycopeptides in addition to Tn-glycopeptides, 237CART cells were tested for the reactivity against LSC, a human colon cancer cell line carries a dysfunctional frameshift mutation in COSMC and also is heavily sialylated from the upregulated expression of ST6GalNAc-I (31). As a positive control for CART activation upon recognizing STn-glycopeptide antigens, I generated the 3H4CAR construct from replacing the scFv of pMP71-5E5-41BB-3z construct with the *scFv* from 3H4, an STn-epitope specific antibody. Karin Schreiber and Frank Wen from Schreiber's lab immunized BALB/C mice with the heavily STn-glycosylated LSC, and generated hybridomas of the antibody producing B cells. 3H4 was screened based on the specific binding to the COSMC-mutant LSC, but not to the COSMC-wildtype LSB which was derived from the same patient. Boris Engels and Christian Idel sequenced the hybridoma to get the coding sequence for 3H4, designed and ordered the pMA-T vector containing the coding sequence for the *scFv* of 3H4 (unpublished). The 3H4-derived CAR specifically recognized LSC very well (**Figure 11**). In contrast, 237CART can be activated by the heavily Tn-glycosylated SKOV3 but not the LSC, indicating it is specifically recognizing Tn- but not STn-glycopeptide antigens in COSMC-mutant cells well (**Figure 11**).

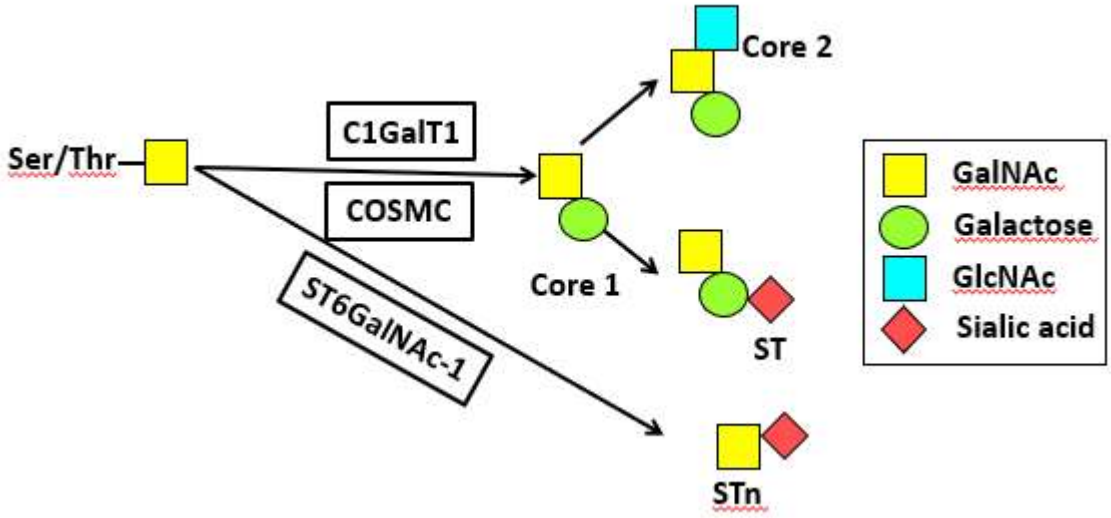

Figure 10. A diagram to show the pathway by which COSMC-mutant cells may acquire STn epitopes from spontaneous high or upregulated activity of ST6GalNAc1 that leads to STn glycosylation of Tn.

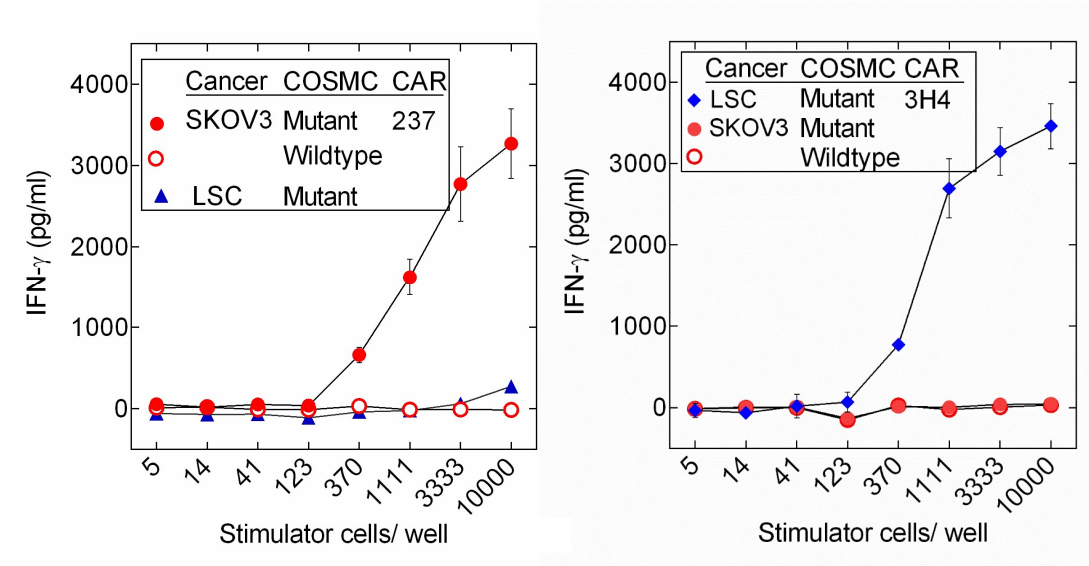

Figure 11. 237CART cells preferentially recognize Tn- rather than STn- glycoepitopes in COSMC-mutant cancers. **Left:** 237CART cells were very sensitive to the Tn-glycopeptide high-expressing SKOV3, but barely activated by the predominately STn-glycosylated LSC. **Right:** The STn-specific-3H4-derived 3H4CART cells were very sensitive to the predominantly STn-glycosylated LSC, but not activated by SKOV3. 10,000 CART cells were co-incubated with either COSMC-mutant or wildtype SKOV3-PDPN, or COSMC-mutant LSC as the stimulator at the indicated number per well for 24h. The level of IFN-γ release into the medium were measured by ELISA (in both panels, n = 2, Mean ± SEM).

Avidity may contribute to but not fully explain the expanded specificity of 237CART

In order to understand the similarities and differences between 237*scFv* used for 237CAR construction and the original 237Ab, I compared the staining of COSMC-mutant or -wildtype cell lines with or without mPDPN expression either with 237*scFv* tetramers* or with 237Ab. (**Figure 12**). As shown in **Figure 12**, 237Ab had no detectable binding to COSMC-mutant cell lines without mPDPN expression at even the highest staining concentration tested (3μM), while a serial 3-fold dilution of 237*scFv* tetramer staining started at 30nM had some very weak signals in cells from Jurkat and Ag104A background and a stronger signal in cells from SKOV3 cells. Otherwise, 237*scFv* tetramer staining had no detectable binding to any of the COSMC-wildtype cell lines just like the original 237Ab.

*The 237*scFv* tetramer-Alexa647 was prepared and shared by Dr. Preeti Sharma from Dr. David Kranz's lab. She also kindly shared with me her tetramer staining protocol

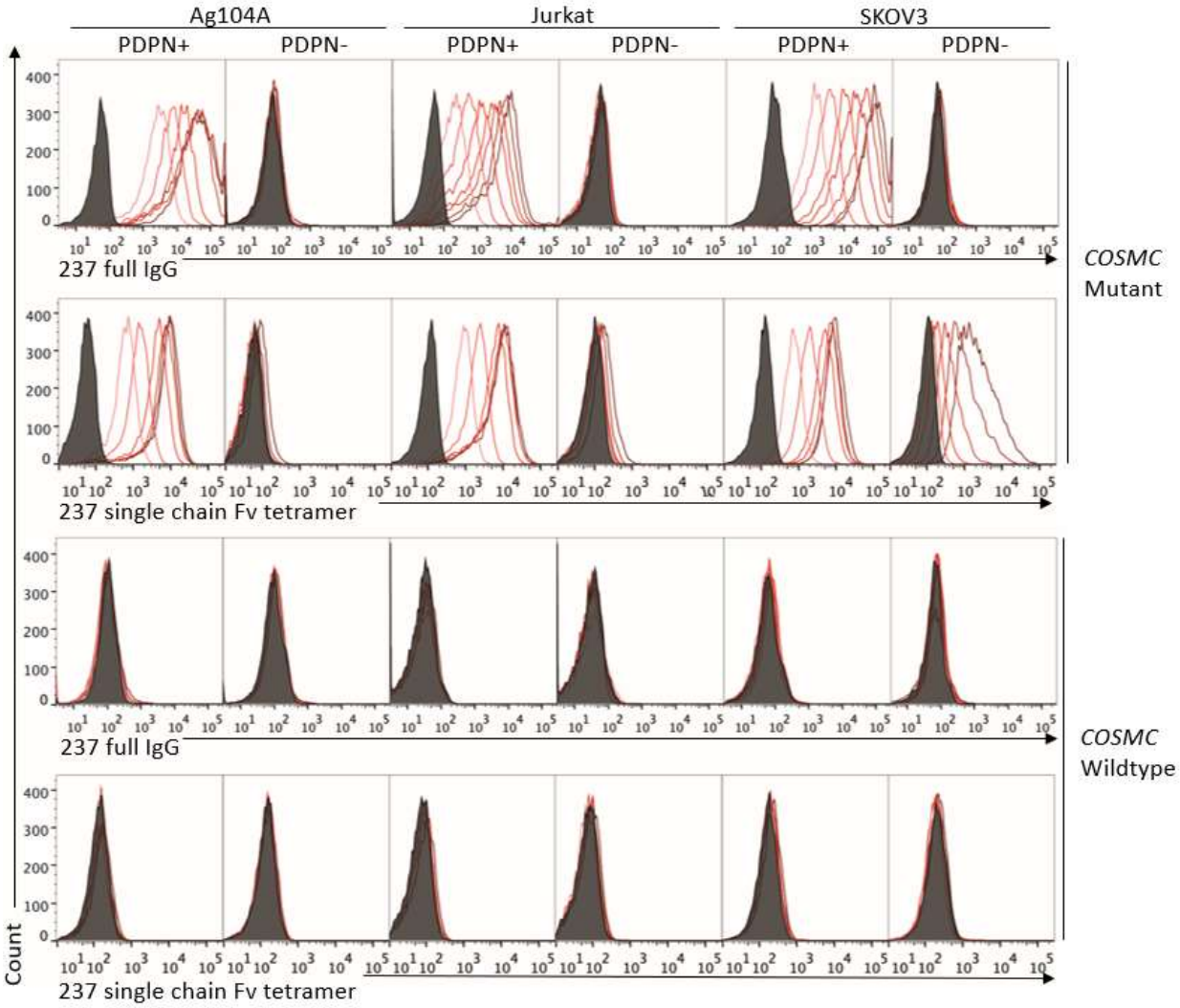

Figure 12. 237Ab and 237*scFv* tetramer staining of COSMC-mutant or wildtype cell lines with or without mPDPN expression. A serial 3-fold dilution of 237Ab started at the concentration of 3μM, or 237*scFv* tetramer* started at the concentration of 30nM were used for staining of cell lines from 3 independent cellular backgrounds. APC $F(ab')_2$ anti-mouse IgG(H+L) was used to detect the primary 237Ab staining at 1:200 dilution. 237*scFv* tetramer staining was evaluated by the Alexa647 linked to the streptavidin.

**The 237*scFv* tetramer-Alexa647 was prepared and shared by Dr. Preeti Sharma from Dr. David Kranz's lab. She also kindly shared with me her tetramer staining protocol

– Discussion

Overall, 237CART recognizes COSMC-mutant cancer cells not predicted by 237Ab staining, while staying safe to normal tissues due to its dependence on the cancer-specific COSMC mutation. Tn-mPDPN stimulated stronger and more durable T-cell responses than that by sub-optimal epitopes not predicted by 237Ab staining, indicating the significance of recognizing the peptide backbone in addition to the dependence on aberrant glycosylation for 237CART activation. Although STn can also be found in COSMC-mutant cancer cell lines, a heavily STn-glycosylated cell line could hardly stimulate 237CART to release cytokines, indicating the specificity of 237CART to Tn rather than to STn antigens in the COSMC-mutant cancer cells. 237*scFv* tetramer staining moderately picked up signals in COSMC-mutant cancer cells that had been missed by 237Ab staining, demonstrating the contribution of avidity effects of 237*scFv* tetramer to the recognition of sub-optimal Tn-glycopeptide epitopes with lower binding affinities in COSMC-mutant cancers by 237CART cells. Therefore, I started the quest for identifying the Tn-glycopeptide motif recognized by 237CART cells, to better understand their specificity when used to treat various type of human cancer cells not expressing mPDPN.

4.2 237CART recognizes multiple different Tn-glycopeptides on a single cancer cell

– Introduction:

It has been shown from crystallography that 237Ab interact with a 7-AA-residue-epitope in mPDPN surrounding the Tn-glycosylated Thr^{77}(45) (**Figure 6**). However, results in my previous chapter have shown 237CART recognition in the absence of mPDPN. Therefore, in this chapter I am going to determine the motif required for 237CART recognition, an extensive panel of alanine (Ala) replacements of the epitope being recognized by 237Ab was chemically synthesized and loaded onto streptavidin-coated plate. The binding of each Tn-mPDPN variant by 237Ab was determined by ELISA, and the recognition of each variant by 237CART cells was determined by the level of cytokine released by the activated T cells. The affinity of 237CAR expressed on T-cell surface to each Tn-mPDPN variant was determined by 2D micropipette measurement. And finally, a panel of multiple different natural Tn-glycopeptide epitopes present in Jurkat leukemia were tested for their capability to activate 237CART cells.

– Results:

237CART recognition is more permissive to aa residue substitutions and truncations of the Tn-glycopeptide epitope than the recognition by 237Ab.

The Tn-mPDPN variants sharing the same *N*-terminal sequence of APLVPTQRERG proceeding the Thr^{77} and the *N*-terminal biotinylation were immobilized on the streptavidin-coated plate at the coating concentration as indicated in the figure legend (**Figure 13**). The binding of immobilized peptides by 237Ab was detected by a traditional sandwich ELISA using anti-mouse IgG-HRP and TMB, and the recognition by 237CART was determined by the level of IFN-γ release by 10,000 237CART upon incubation with immobilized peptides for 24 h. **Figure 13** (**upper panels**) shows that the Tn on Thr^{77} of mPDPN is essential for 237Ab binding and 237CART activation. Binding of the 237Ab to peptide-coated plates was significantly reduced when the Gly^{76} was replaced with an Ala, and single Ala replacement of two other aa residues caused a small reduction. However, none of the single Ala replacements significantly reduced the activation of 237CART alone. I therefore proceeded to multiple Ala replacements (**Figure 13, middle panels**). Surprisingly, even replacement of all 5 aa residues into Ala was permitted for 237CART activation. If, however, the Gly^{76} was also replaced by an Ala, 237CART activation was then compromised considerably. This contrasts the 237Ab binding which was already significantly diminished after substitution of the Gly76 alone. Since up to 4 of the 5 C-terminal aa residues can be replaced by Ala without significantly compromising the activation of 237CART, I further investigated what was the minimal length of the C-terminal peptide required for 237CART activation. (**Figure 13, lower panels**), shows that the shortening of the peptide always had a more significant influence on 237Ab binding than that on 237CART activation, while the reduction of up to 2aa residues

from the C-terminus could still be tolerated by 237CART. The above experiments demonstrate a greater permissiveness of 237CART activation than 237Ab binding to Ala replacements and shortening of the 237Ab binding motif within the mPDPN.

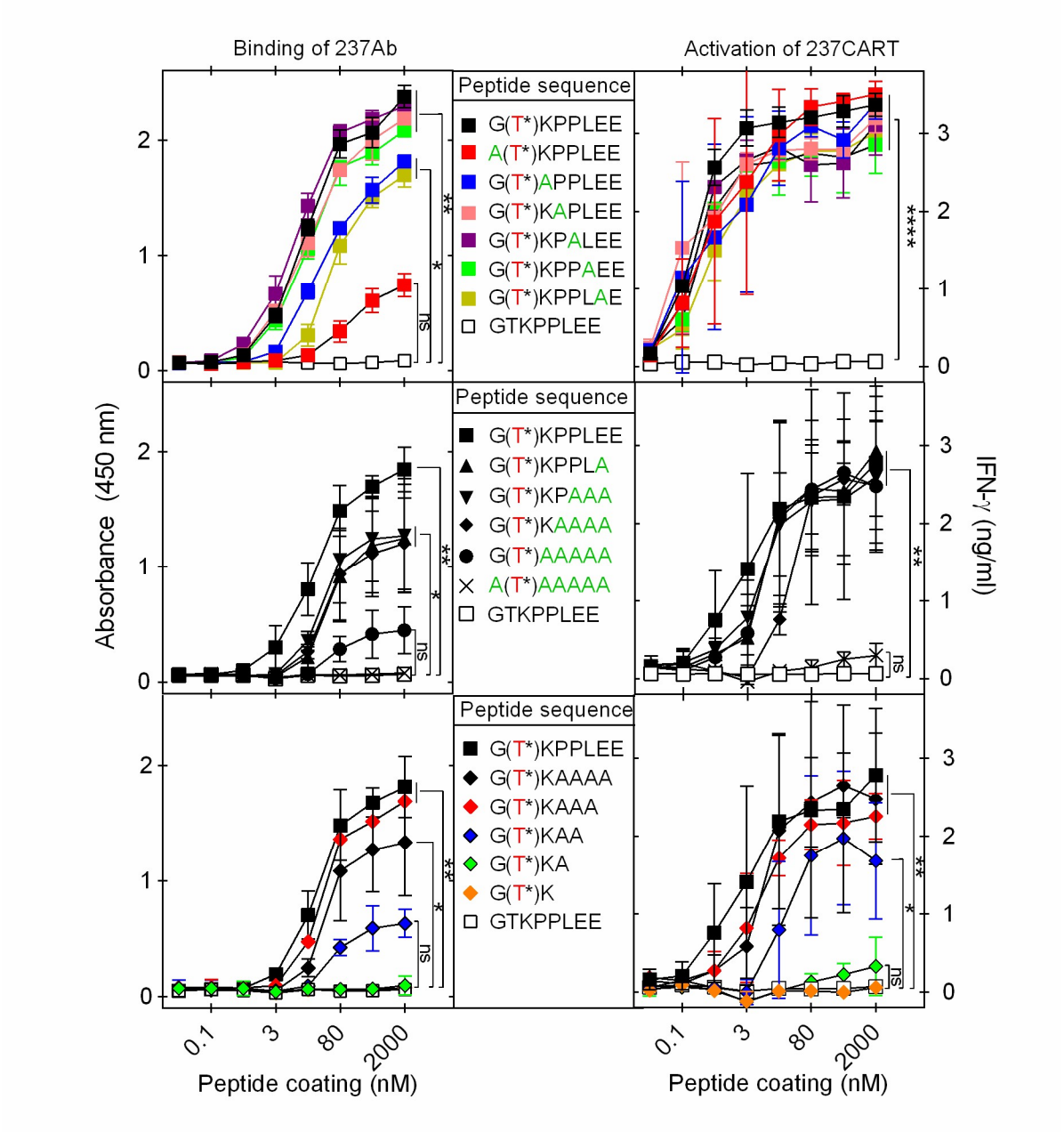

Figure 13. 237CART recognition is more permissive to aa residue substitutions and truncations of the Tn-glycopeptide epitope than the recognition by 237Ab. Peptides started with the common mPDPN sequence of APLVPTQRER were immobilized onto streptavidin-coated plates at the coating concentration as indicated via the common *N*-terminal biotinylation.

Figure 13, continued. The Tn-glycosylated Thr^{77} of mPDPN was labeled in **red**, while the Ala replacements of the original mPDPN sequence labeled in **green**. 50μg/ml 237Ab binding to the immobilized peptides was quantified by anti-mIgG-HRP and TMB; while the activation of 237CART was evaluated by the level of IFN-γ released after 24 h incubation of 237CART with immobilized peptides detected by the sandwich ELISA. **Upper panel:** Ala scanning of the 237Ab binding epitope with one aa residue replacement at a time. **Middle panel:** Ala scanning of the 237Ab binding epitope with an increasing number of aa residues at a time. **Lower panel:** Gradual shortening of the 237Ab binding epitope from the C-terminus. The gradual shortening increasingly compromised both 237Ab binding and 237CART recognition, often causes more significant damage to 237Ab binding than that to 237CART activation. The statistical significance of the differences between two groups as pointed out by the brackets was calculated by Student's t-test. Mean ± SEM, n = 3.

Single Ala replacements of aa residues within the Tn-mPDPN epitope recognized by 237Ab made no discernible differences in the 2D affinity measurement by 237CART

A micropipette adhesion frequency assay measures the cell-to-cell interaction between a CART and an artificial APC, in this case, a streptavidin-coated RBC loaded with biotinylated Tn-mPDPN variants with a single Ala replacement* of every aa residues within the epitope in mPDPN being recognized by 237Ab. Results show that none of the single Ala replacements within the Tn-mPDPN epitope had made any significant difference to the 2D affinity of the Tn-glycopeptide variant recognized by 237CART. The diagram of the assay is depicted in **Figure 14**. A 237CARGFP T-cell captured by a micropipette was repeatedly forced to touch the RBC loaded with one type of the Tn-PDPN single Ala replacement for a certain duration of period (contact time 0.25, 0.5, 0.75, 1, 2, and 5 s). Adhesion events were defined by the elongation of RBC upon cell separation which were recorded manually by observation during the 50 repeated contact-retract cycles. Unglycosylated PDPN was used for subtracting the non-specific binding background. The results of the measurements are shown in **Figure 15** and **Table. 4**

*The 237CART cells were prepared by Yanran He, the biotinylated RBCs were prepared by Yanran He with the help from Jill Rosenberg from Dr. Jun Huang's lab, the 2D measurement assay and data analysis was performed by Dr. Wei Feng from Dr. Jun Huang's lab.

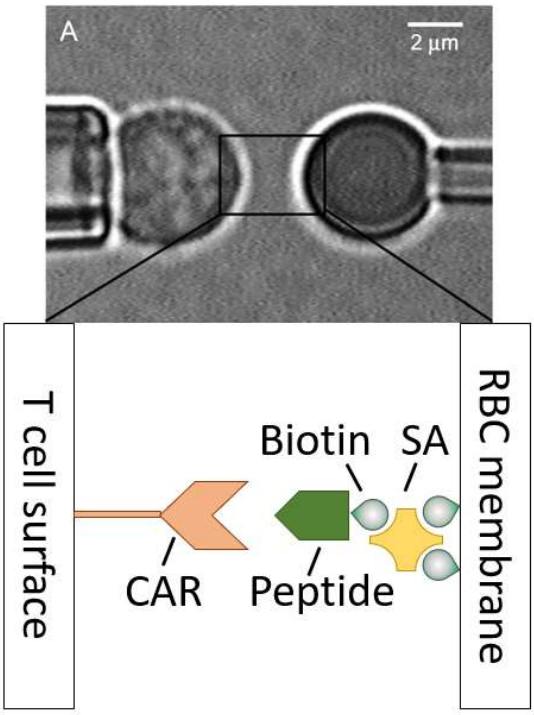

Modified from Jiang, N. *et al.* . *Immunity* **34,** 13–23 (2011)

Figure 14. A diagram for a micropipette adhesion frequency assay performed using a CART recognizing ligands loaded on an RBC. The left side showing a micropipette is holding a T-cell, while the right side showing a micropipette is holding an RBC loaded with target peptides. A T-cell captured by a micropipette was repeatedly forced to touch the RBC loaded the target peptide for a certain duration of period (contact time 0.25, 0.5, 0.75, 1, 2, and 5 s). Adhesion events were defined by the elongation of RBC upon separation which were recorded manually by observation during the 50 repeated contact-retract cycles. Unglycosylated PDPN was used for subtracting the non-specific binding background.

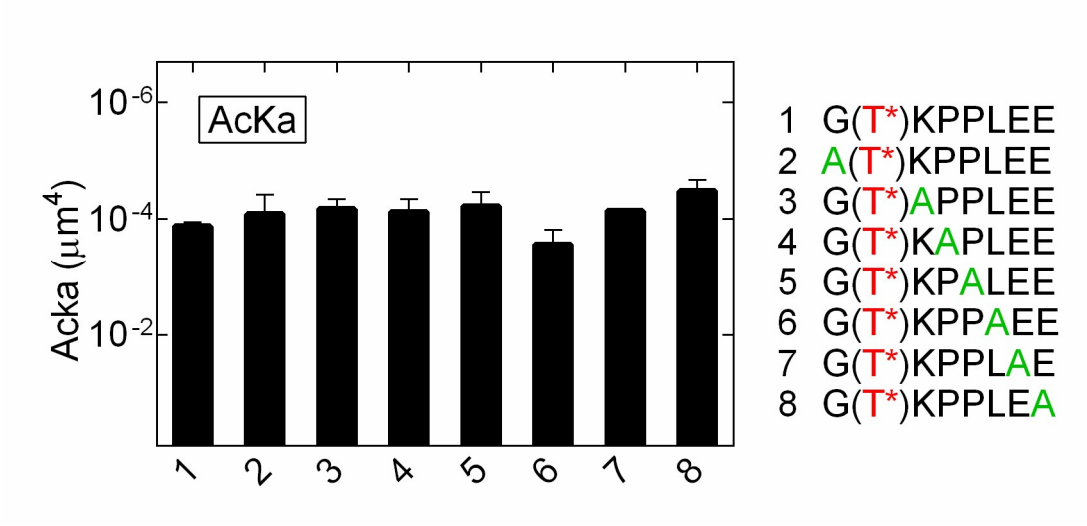

Figure 15. 2D Affinity measurements* of 237CART binding to different Tn-mPDPN variants with a single Ala replacement. A 237CARGFP-transduced T-cell captured by a micropipette was repeatedly forced to touch an RBC loaded with either one type of the Tn-PDPN single Ala replacement variants as that mentioned in the list (contact time 0.25, 0.5, 0.75, 1, 2, and 5 s). Adhesion events are defined by the elongation of RBC during cell separation and were recorded manually by observations during the 50 repeated contact-retract cycles. Unglycosylated PDPN was used for subtracting the non-specific binding background.

---

*The 237CART cells were prepared by Yanran He, the biotinylated RBCs were prepared by Yanran He with the help from Jill Rosenberg from Dr. Jun Huang's lab, the 2D measurement assay and data analysis was performed by Dr. Wei Feng from Dr. Jun Huang's lab.

Table 4. 2D affinity measurement of 237CAR to Tn-PDPN single Ala replacement

Peptide	$A_c k_a$ (μm^4)	k_{off} (s^{-1})	AcKon ($\mu m^4 s^{-1}$)
Biotin-APLVPTQRERG(T*)KPPLEE	1.3 ± 0.2 (× 10^{-4})	1.2 ± 0.4	1.5 ± 0.4 (× 10^{-4})
Biotin-APLVPTQRERA(T*)KPPLEE	8.1± 4.3 (× 10^{-5})	1.6 ± 0.1	1.3 ± 0.7 (× 10^{-4})
Biotin-APLVPTQRERG(T*)APPLEE	6.7 ± 2.1 (× 10^{-5})	1.4 ± 0.2	9.2 ± 3.2 (× 10^{-5})
Biotin-APLVPTQRERG(T*)KAPLEE	7.4 ± 2.9 (× 10^{-5})	1.6 ± 0.6	1.1 ± 0.3 (× 10^{-4})
Biotin-APLVPTQRERG(T*)KPALEE	5.9 ± 2.5 (× 10^{-5})	1.9 ± 0.7	1.0 ± 0.2 (× 10^{-4})
Biotin-APLVPTQRERG(T*)KPPAEE	2.7 ± 1.2 (× 10^{-4})	2.2 ±1	5.6 ± 3.6(× 10^{-4})
Biotin-APLVPTQRERG(T*)KPPLAE	7.2±7.4 (× 10^{-5})	2 ± 1.4	1.0 ± 0.7 (× 10^{-4})

*The 237CART cells were prepared by Yanran He, the biotinylated RBCs were prepared by Yanran He with the help from Jill Rosenberg from Dr. Jun Huang's lab, the 2D measurement assay and data analysis was performed by Dr. Wei Feng from Dr. Jun Huang's lab.

237CART cells recognize multiple different Tn-glycopeptide Ags on a single cancer cell

A panel of different Tn-glycopeptides epitope that have been found to be naturally present in Jurkat (57) were chemically synthesized with N-terminal biotinylation and were tested for binding by 237Ab and recognition by 237CART cells. The Tn-glycopeptides were immobilized on the streptavidin-coated plate and were tested for binding by 237Ab or recognition by 237CART cells as described in **Figure 13**. **Figure 16** shows 237Ab only exhibited detectable binding to Tn-mPDPN but not to any other Tn-glycopeptides that were naturally presented on the surface of Jurkat cells, whereas 237CART reacted with several different Tn-glycopeptides regardless of distinct peptide sequences compared to Tn-mPDPN.

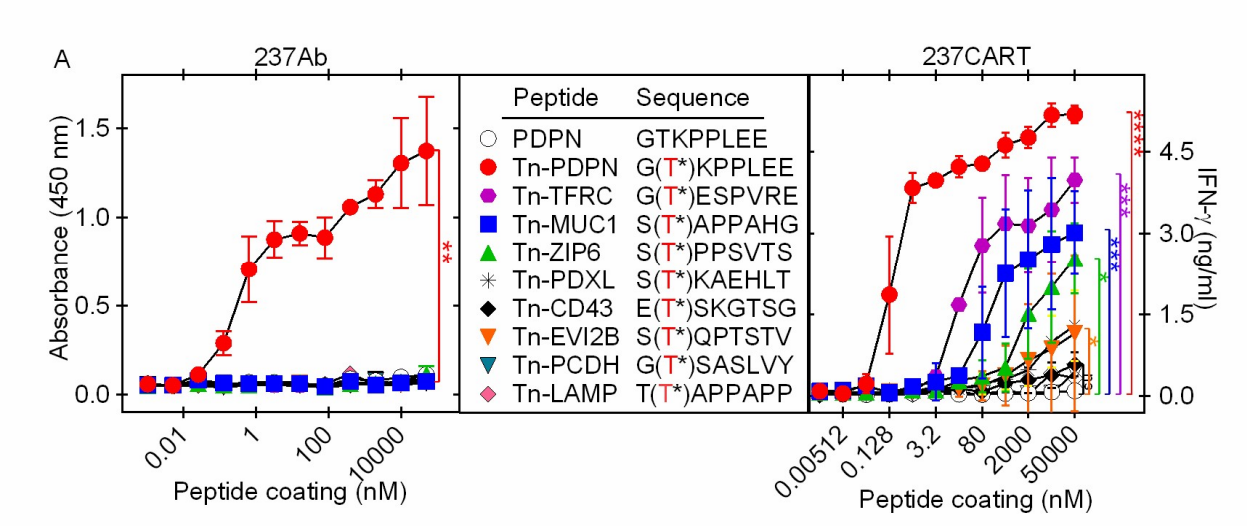

Figure 16. 237Ab binding and 237CART activation upon recognition of Tn-glycopeptide epitopes naturally presented in Jurkat cells. A panel of biotinylated Tn-glycopeptides were immobilized on streptavidin coated plate at the coating concentration as indicated. On the **Left**, 237Ab was added to the plate at 50 μg/ml in coating buffer and the binding of which was detected by anti-mouse IgG-HRP and TMB. On the **Right**, 10,000 237CART cells were added to each well of peptide-coated plate and incubated for 24h. 237CART activation was evaluated by cytokine release into the medium. The statistical significance of the differences between two groups as pointed by the bracket was calculated by Student's t-test. Mean ± SEM, n = 3.

– Discussion:

237CART recognized several different Tn-glycopeptides naturally present in Jurkat cells not predicted by 237Ab binding. The results demonstrated the wide coverage of 237CART in recognition of multiple different cancer-specific Ags on a single human cancer cell. The simultaneous targeting of multiple different antigens should minimize the possibility of cancer relapse, because a spontaneous repair of the loss-of-function mutation would be highly unlikely. It has been previously discussed that proteins such as enzymes and antibodies may have polyfunctional combining regions for recognition of structurally related ligands (58, 59). Furthermore, the sensitivity of recognition by CART may further enhanced through the avidity effect. The recognition of antigens expressed on normal tissues even at extremely low levels could be problematic for CART as this could lead to serious toxicity (12, 60). Fortunately, in the case of 237CART, the cross-reactivity has only been detected with other Tn-glycopeptide antigens which makes the recognition still highly cancer-specific, and the extended specificity to recognize a wide-range of Tn-glycopeptides minimizes potential cancer relapses by simultaneously targeting multiple different targets on a cancer cell.

4.3 The *in vivo* efficacy of 237CART cells in treating hematopoietic and solid tumors

- Introduction

237CART has exhibited a broad reactivity with multiple different human COSMC-mutant cancers not restricted by mPDPN expression in the previous chapters. In this section of the study, I will test 237CART for its capability of treating human and mouse leukemia or solid tumors. Specifically, I will compare the efficacy of 237CART with the clinically-proven CD19CART in treating a systemic Jurkat leukemia transplanted in the NSG mouse model. In addition, I will compare the efficacy of 237CART in treating several different types of solid tumors and discuss the promises and challenges of applying 237CART to treat leukemia and solid tumors.

– Results

237CART completely eradicated established Jurkat leukemia in the presence or the absence of mPDPN dependent on COSMC-mutation

To compare the *in vivo* efficacy of 237CART to that of CD19CART cells which have eradicated established leukemia in patients (61), I have tested the therapeutic efficacy of 237CART treating a 14-day-old established systemic Jurkat leukemia in NSG mice transplanted via tail vein injection. Jurkat is a human T-cell leukemia with a spontaneous COSMC mutation that leads to loss-of-function of COSMC (30). It is not expressing mPDPN nor human CD19. 237CART treatment completely eradicated mPDPN-transduced Jurkat leukemia as that of CD19CART treating CD19-transduced Jurkat-COSMC wildtype. (**Figure 17, left and middle**). Surprisingly, 237CART also eradicated COSMC-mutant Jurkat transplant in the absence of mPDPN expression (**Figure 17, right**). The results supported the broad reactivity of 237CART with COSMC-mutant human cancers and not dependent on mPDPN expression, which opens many possibilities of applying 237CART for the treatment of multiple different human cancers.

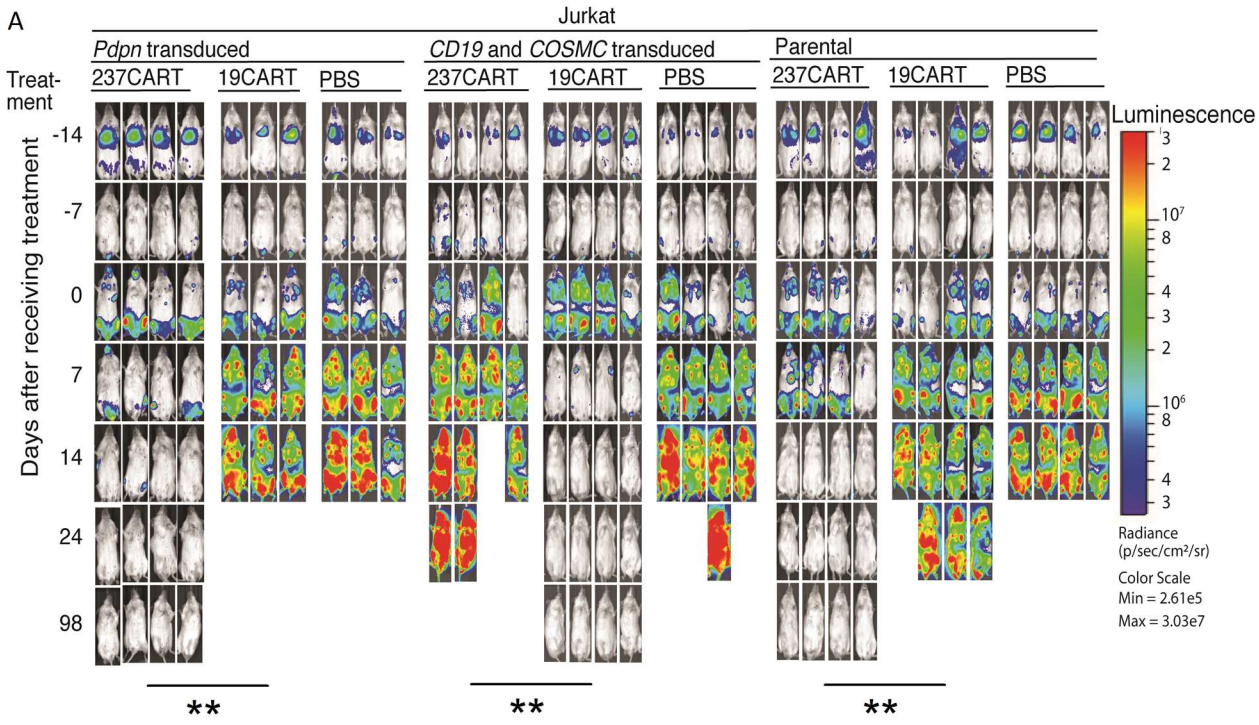

Figure 17. 237CART eradicated Tn-glycopeptide expressing human cancers not predicted by 237Ab binding. The survival of NSG mice bearing 2-week-old established systemic Jurkat leukemia (5 million of either *Pdpn*-transduced, *COSMC*-wildtype and *CD19*-transduced, or the parental Jurkat transplanted through tail vein injection) were treated with either 2 million 237CART or CD19CART, or PBS mock treatment through intraperitoneal injection. The disease progression was monitored by live animal bioluminescence imaging (n = 4 or 3 mice per group as indicated in the figure). The significance level of the difference between the survival of animals from different treatment groups was determined by log-rank Mantel-Cox test. ** indicates $p < 0.01$

237CART eradicated Jurkat subcutaneous transplant

The first solid tumor model I have tested was the original Jurkat cancer cells without mPDPN, injected subcutaneously to grow into solid tumors. 10 million Jurkat cells were transplanted in two NSG mice and both formed solid tumor (**Figure 18**). Both animals were treated with 2 million 237CART cells when the Jurkat tumor reached around 200-300 mm^3, and both tumors regressed significantly. However, one of the two animals treated relapsed shortly after and the tumor growth progressed very fast. Therefore, I gave a second and a third dose of 2 million 237CART each time to the animal. Luckily, the additional two treatments completely rejected the large (closed to 1000 mm^3) relapsed tumor and the animal remained disease-free throughout the time of follow-up (> 100 days), indicating early promises of treating the large solid tumors. Nevertheless, the observation requires further validation in more independent repeats, and I have tested if the success could be replicated in other cancer types as well.

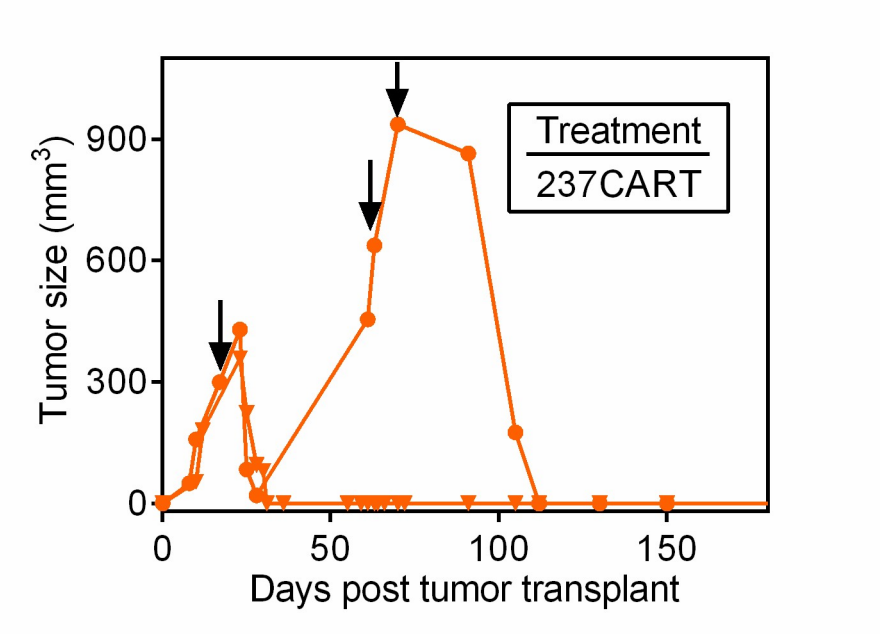

Figure 18. Treatment of Jurakt subcutaneous transplantations with 237CART cells. 2 mice were transplanted with 10 million Jurkat leukemia cells subcutaneously. 2 weeks later, each mouse received 2 million 237CART treatment. After the tumor in one animal relapsed, 2 additional doses of 237CART cells of 2 million each was given at the time point as indicated only to the mouse with the relapse. The tumor growth was monitored by measuring each tumor's dimensions using a caliper.

237CAR controlled COSMC-mutant SKOV3 tumor growth in vivo in the presence but not in the absence of mPDPN

Previous findings have shown that Jurkat subcutaneous transplants can be treated with 237CART cells. The results encouraged me to further investigate the efficacy of 237CART in treating cells from solid tumor backgrounds. SKOV3 subcutaneous transplant in B6xRag1$^{-/-}$ has been previously reported to be responding to anti-Her2CART treatment (62). I tested whether 237CART cells could specifically recognize COSMC-mutant SKOV3 in the presence or absence of mPDPN expression. As shown in **Figure 19**, 237CART successfully eradicated Tn-mPDPN expressing SKOV3 tumor transplant, but not COSMC-mutant SKOV3 tumors lacking mPDPN expression. The result suggested the complete eradication of some solid tumor types would require potent T-cell activation that might not be achieved in the absence of Tn-mPDPN expression.

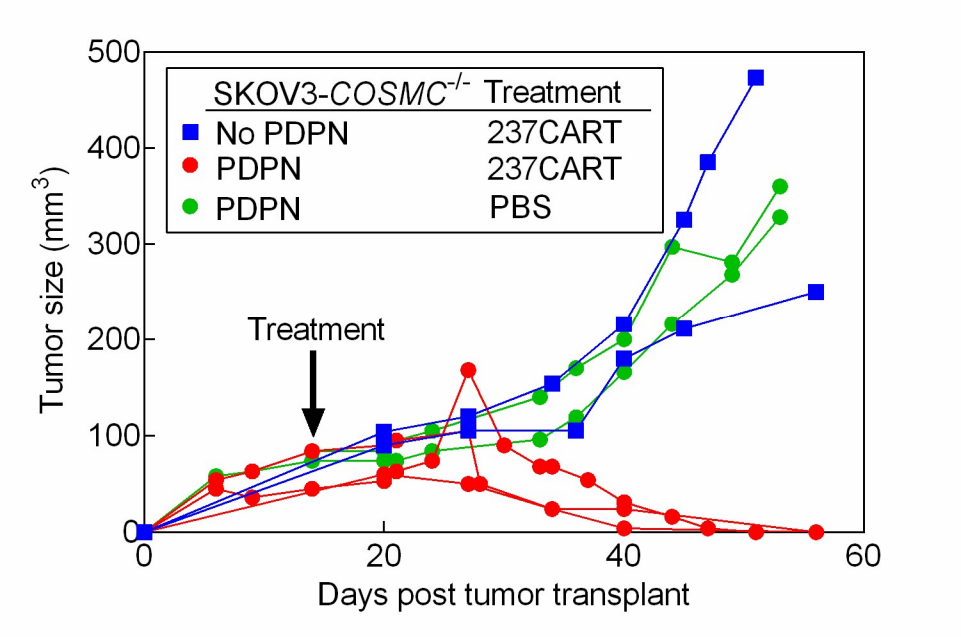

Figure 19. Responses of SKOV3 COSMC-mutant tumors to 237CAR T-cell treatment. Five million SKOV3 cells of each variant as indicated in the figure legend were injected subcutaneous in B6Rag1$^{-/-}$. Two weeks later, the mice were either treated with 2 million 237CART cells, or PBS mock treatment. Tumor growth was monitored by dimension measurements. Two animals in each treatment group.

237CAR could not control COSMC-mutant Ag104A tumor growth in vivo even in the presence Tn-mPDPN

Ag104A is a murine sarcoma with a loss-of-function COSMC mutation, and naturally expresses a high level of mPDPN. In a preliminary experiment, I have tested the efficacy of 237CART for treating Ag104A COSMC-mutant or -wildtype tumors in one animal each and found 237CARTcells could not slow down the growth of Ag104A compared to Ag104A-COSMC-wildtype (**Figure 20**), although Ag104A stimulated strong 237CART activation *in vitro* (**Figure 8**), the tumor progressed almost as fast as Ag104A-COSMC-wildtype (**Figure 20**) which could not stimulate 237CART activation (**Figure 8**). The conclusion needs to be further validated by further repeats as only one animal of each treatment group was used. Next I determined whether treating Ag104A at a smaller size would make the treatment more effective. To this end, one mouse was treated when the tumor is around ~400 mm^3, while the other animal received 237CART treatment when the tumor was only around 100 mm^3, to see whether tumor arrest can be achieved by 237CART treatment. However, even the smaller tumor at the point of treatment progressed very fast after receiving the 237CART cells (**Figure 21**).

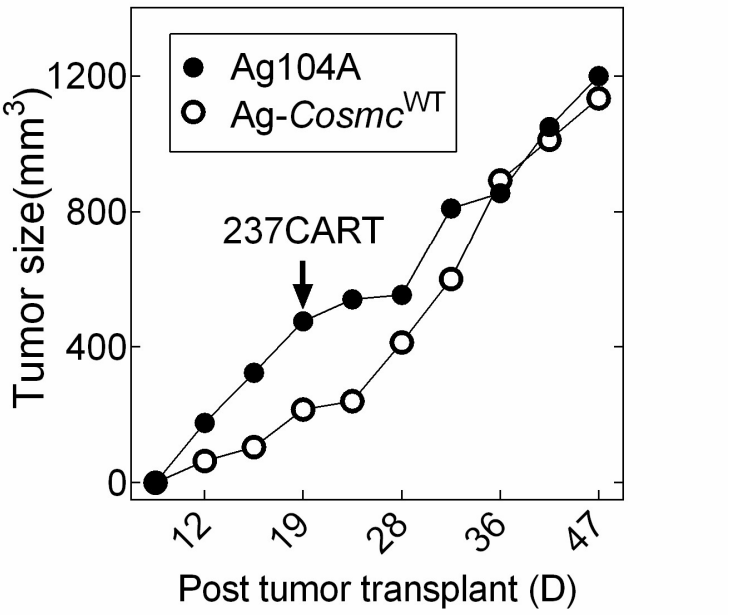

Figure 20. 237CART could not suppress the outgrowth of Ag104A tumors. Half a million COSMC-mutant or wildtype Ag104A cells were injected s.c. in B6Rag1$^{-/-}$mice. Both mice were treated with 2 million 237CART cell 19 days after tumor transplant. Tumor growth was measured by a caliper. One mouse received transplantation of one type of tumor

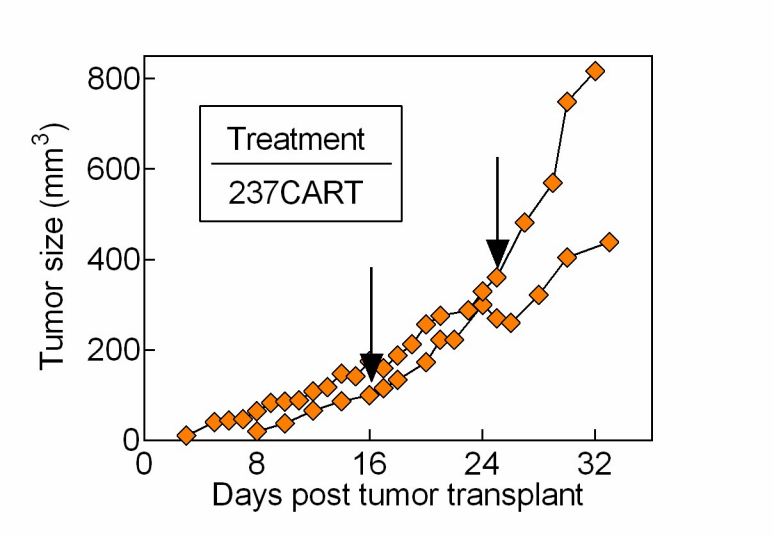

Figure 21. 237CART cells could not suppress the outgrowth of even small Ag104A tumors. Half a million Ag104A cells were injected s.c. into B6Rag1$^{-/-}$. Either 16 or 24 days later, when the tumor was around either 100 mm^3 or 400 mm^3 in size, each mouse received 2 million 237CART cells i.p. Tumor growth was monitored by measuring the dimensions using a caliper. 1 animal in each group.

Together, my results show that there is no difference in the growth curve of the Ag104A tumors whether being treated early or late. I further determined whether the tumor microenvironment of Ag104A was suppressing the tumor-reactive T cells. To this end, I isolated TILs from Ag104A and from Ag104A-COSMC-wildtype treated with 237CART. The number of TIL, the tumor reactivity of the TILs compared to that of 237CART freshly transduced was determined (**Figure 22**).

First of all, there was a very few TILs that can be isolated from either Ag104A or the Ag104A-COSMC-wildtype when compared to that that can be isolated from the majority of other solid cancer types (~ $1x10^5$ vs several million from per approximately 100 mm^3 of tumor tissue**)**, indicating there might already has been an barrier that prevented the tumor-reactive T cells to get into the tumor. Second, the activity and the specificity of the TILs isolated were tested for cultured cancer cells and SIINFEKL peptides, and the results revealed the significantly compromised activity of the TILs compared to that of the freshly transduced-T cells. Therefore, ACT for Ag104A would require novel strategy to break the immune suppression in the tumor microenvironment.

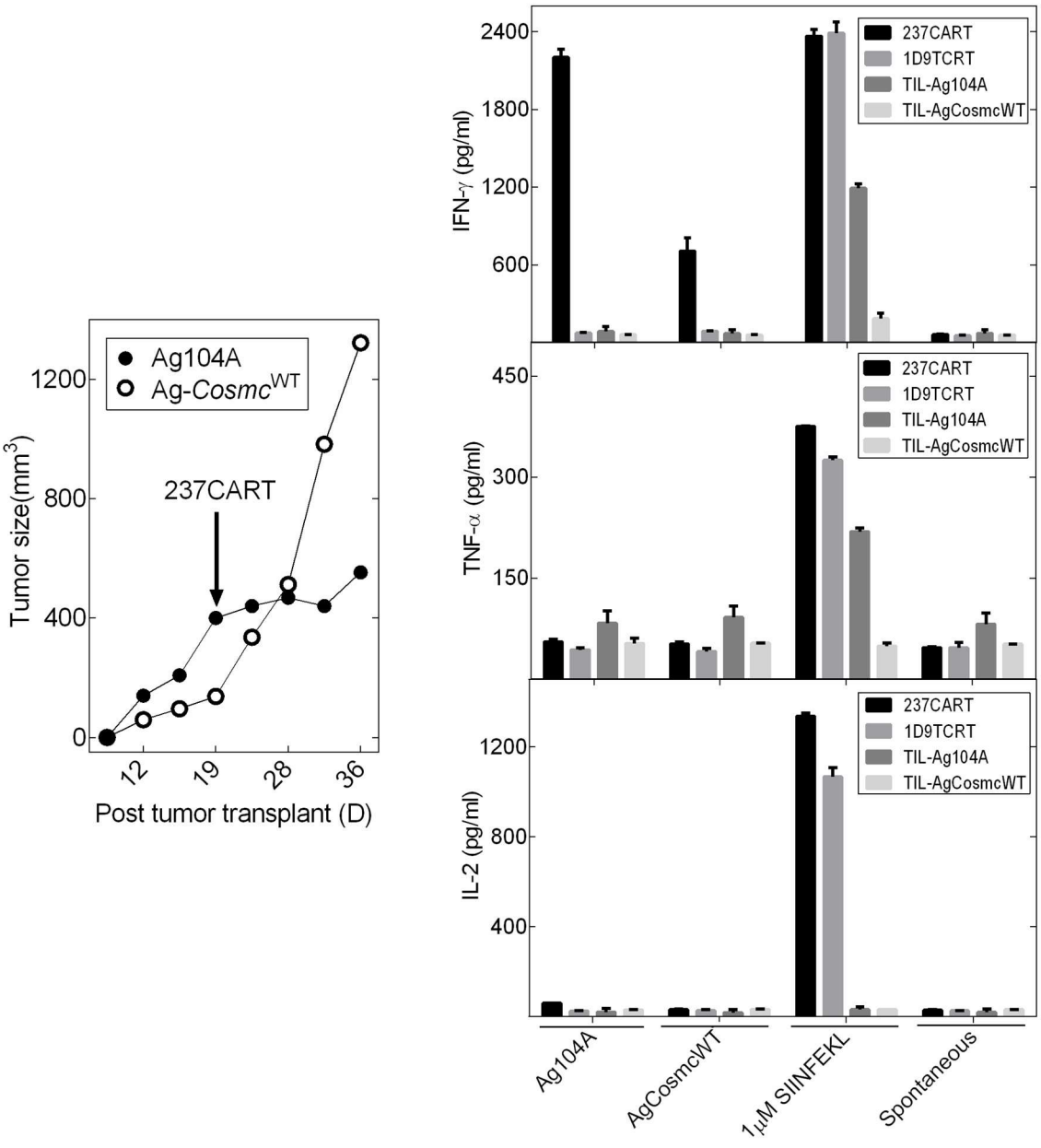

Figure 22. The activity of TILs isolated from Ag104A and Ag104A COSMC-wildtype tumors. Half a million Ag104A or Ag104ACOSMC-wildtype tumor cells were transplanted s.c. and received 2 million 237CART treatment 19 days after tumor transplant. 2 weeks later, TILs were isolated from tumor tissue using anti-mouse CD8a MACS column, and the isolated T cells (10,000 per well) were tested for the level of cytokine release into the medium upon 24 h co-incubation with 10,000 Ag104A or Ag104ACOSMC-wildtype cancer cells. Stimulation by 1μM SIINFEKL peptide and the plain T-cell culture medium were used as the positive and negative controls respectively. IFN-γ, TNF-α, and IL-2 cytokine release levels were determined by sandwich ELISA.

The combination of a cancer-targeting CD8$^+$ CART and a stroma-targeting CD4$^+$ TCRT failed to eradicate Ag104A tumor transplants

CART cells only recognize antigens on the surface of cancer cells, while it could be critical for the cells to also target the stroma in order to modulate cancer microenvironment. To fully realize the potential of adoptive T-cell transfer therapy for treating solid tumors, a class II antigen, mutant ribosomal protein L9 (mRLRP9), was introduced to Ag104A by retroviral transduction which can be recognized by 479-H60 TCR (46). To determine whether the combination of a cancer-targeting 237CAR- CD8$^+$ T-cell treatment with a stroma-targeting 479-H60TCR- CD4$^+$ T-cell treatment could arrest the Ag104A solid tumor growth, I transplanted half a million Ag104A-mRLRP9 tumors s.c. in two C3HRag2$^{-/-}$ mice, which both have Class II HLA E^k in the stroma to present mRLRP9 Ag to be recognized by 479H60 TCR. Both mice received the combinational treatment of 237CAR-transduced CD8$^+$ T cells from the splenocytes of OTIxRag1$^{-/-}$ mice, and 479H60TCR-transduced CD4$^+$ T cells from the splenocytes of C3HCD8$^{-/-}$ mice. The treatment seemed to have caused a moderate regression in the tumor growth in both mice (**Figure 23**). However, the experiment is lacking a critical control of the treatment by 479H60TCR-transduced CD4$^+$ T cells treatment only, making it hard to tell whether the combination really made a difference to the treatment by 479H60-CD4$^+$ or 237CAR-transduced CD8$^+$ T-cell treatment alone. Therefore, the preliminary observation shall be validated in further repeats in comparison to the efficacy by the 479H60-CD4$^+$ or 237CAR-transduced CD8$^+$ T-cell treatment alone.

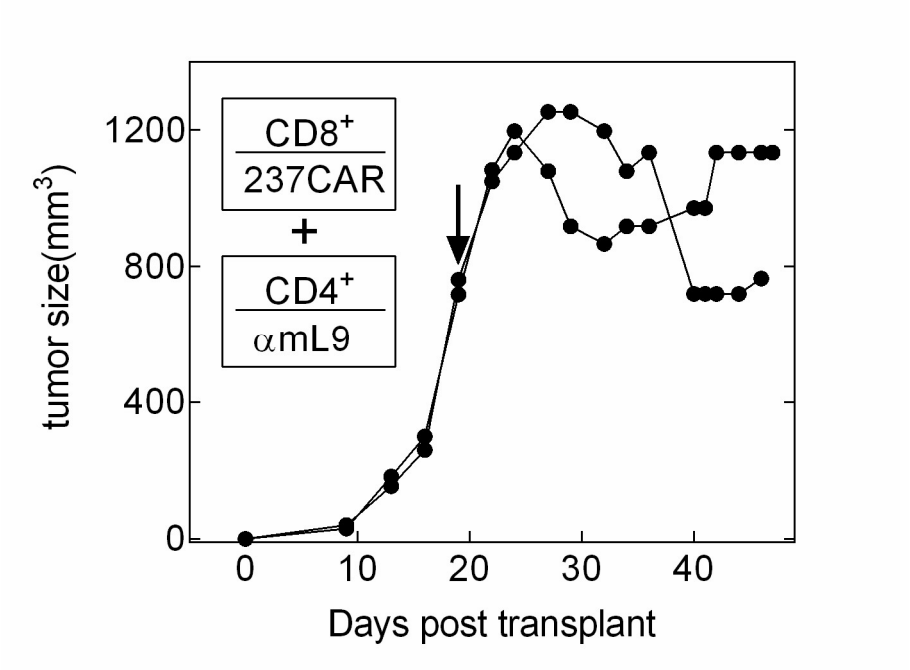

Figure 23. Responses of Ag104A-mRLRP9 to the combinational treatment of 237CAR-CD8$^+$ T cells and 479H60TCR-CD4$^+$ T cells. Half a million Ag104A-mRLRP9 were transplanted in C3HRag2$^{-/-}$ mice, the mRLRP9 is an MHC class II-presented antigen which can be targeted by 479H60TCR-CD4$^+$ T cells, and the Tn-mPDPN antigen can be targeted by 237CAR-CD8$^+$ T cells. The tumor growth in mice received combinational treatment at 19 days after tumor transplantation were monitored by dimensions measured by a caliper. There were two mice in this treatment group.

– Discussion:

In this chapter, I have demonstrated the broad reactivity of 237CART recognizing Tn-glycopeptide Ags not predicted by 237Ab binding. This reactivity was sufficient to mediate complete rejection of 2-week-old systemic Jurkat transplant. The recognition of antigens not predicted by 237Ab binding was sufficient to reject established leukemia free of relapses. Possibly, 237CART cells benefited from simultaneous targeting multiple different Tn-glycopeptide antigens on the cancer cell.

The 237CART treatment also worked for Jurkat s.c. transplants, for a tumor as big as 1000 mm^3, after repeated dosing of 237CART treatments. While cancer cells often circumvent recognition by ACT by loss of antigen expression(8), the dependence of 237CART recognition on a loss-of-function makes it unlikely suffer from the unstable antigen expression because the loss-of-function mutation is unlikely to be spontaneously repaired. The treatment may be further improved by novel CART construct/manufacturing protocol that makes the functional T cells more resistant to exhaustion (10).

The T-cell activation in recognition of COSMC-mutant cancers was always stronger in the presence of Tn-mPDPN, while there was a smaller difference between the mPDPN-positive vs -negative groups in their ability to induce target lysis than that to induce cytokine releases. Although it has been reported that both target lysis and cytokine release can be mediated by single digit TCR engagements (63, 64). The stable generation of cytokines may require a higher threshold for activation than that for the lytic activity (65). The T-cell activation by suboptimal mimotope engagements may not be able to reach the threshold for stable activation of critical T-cell functions for eradications of solid tumors.

The successful treatment of COSMC-mutant SKOV3 with mPDPN expression with 237CART showed the promise of using 237CART to treat solid tumors. The inability of 237CART to induce effective rejection of COSMC-mutant SKOV3 without PDPN expression indicates the importance of fully activated CART for rejection of solid tumors. To this end, the specificity of 237*scFv* can be engineered towards Tn-glycopeptide Ags commonly found in human cancers to improve the potential efficacy.

The failed attempts of treating Ag104A have told us a solid tumor can be quite resistant to CART treatments. Tumor-reactive T cells may have difficulties in getting into the tumor microenvironment, which can be improved by combinational use of immune-modulating drugs as well as CD4 T cells recognizing the tumor microenvironment (66-68).

4.3 A new paradigm of targeting multiple cancer-specific Tn-glycopeptides by a single CAR

– Introduction

Having demonstrated the simultaneous targeting of multiple cancer-specific Tn-glycopeptide Ags by a single CAR derived from a Tn-glycopeptide specific Ab 237. I further investigated whether the principal would apply to other Tn-glycopeptide specific antibodies as well. Therefore, I have tested the activity and specificity of 5E5CAR-transduced T cells (5E5CART), engineered with a CAR derived from a mouse monoclonal Ab 5E5, generated from immunization of a mouse with synthesized Tn-MUC1 and has been shown to react to Tn-MUC1 (19, 69). The 5E5CART has previously been demonstrated to recognize targets expressing Tn-MUC1 (47), here I am testing whether 5E5CART would cross-react with other Tn-glycopeptides like 237CART does, using multiple different human and murine cancer cell lines either COSMC-mutant or wildtype, with or without human MUC1 expression. In addition, I have tested the activity of 5E5CART in recognition of a panel of synthesized Tn-glycopeptides replicating the natural Tn-glycosylated epitopes found in Jurkat leukemia.

– Results

5E5CART recognizes COSMC-mutant cancers not expressing MUC1

As a test for the generality of our observation that whether a CAR derived from a Tn-glycopeptide-specific Ab would react with other Tn-glycopeptide not predicted by the Ab binding, I examined 5E5CART derived from 5E5Ab, which was generated from immunizing a mouse with Tn-glycosylated human mucin 1 (Tn-MUC1) (19, 69). In (**Figure 24**, **upper panel**) 5E5CART recognized Tn-mPDPN as well, but not other Tn-glycopeptides tested. This indicates 5E5CART can also recognize more Tn-glycopeptides than that can be predicted by 5E5Ab binding. The pattern of cross-reactivity was however different between 237CART and 5E5CART, since 5E5CART was not activated by some Tn-glycopeptides that activated 237CART. 5E5CART not only killed cancers expressing Tn-MUC1 as it has been reported (47), but it also recognized COSMC -mutant cancers that did not express MUC1 (**Figure 24**, **lower panel**), supporting the generality of our discovery made with 237CART.

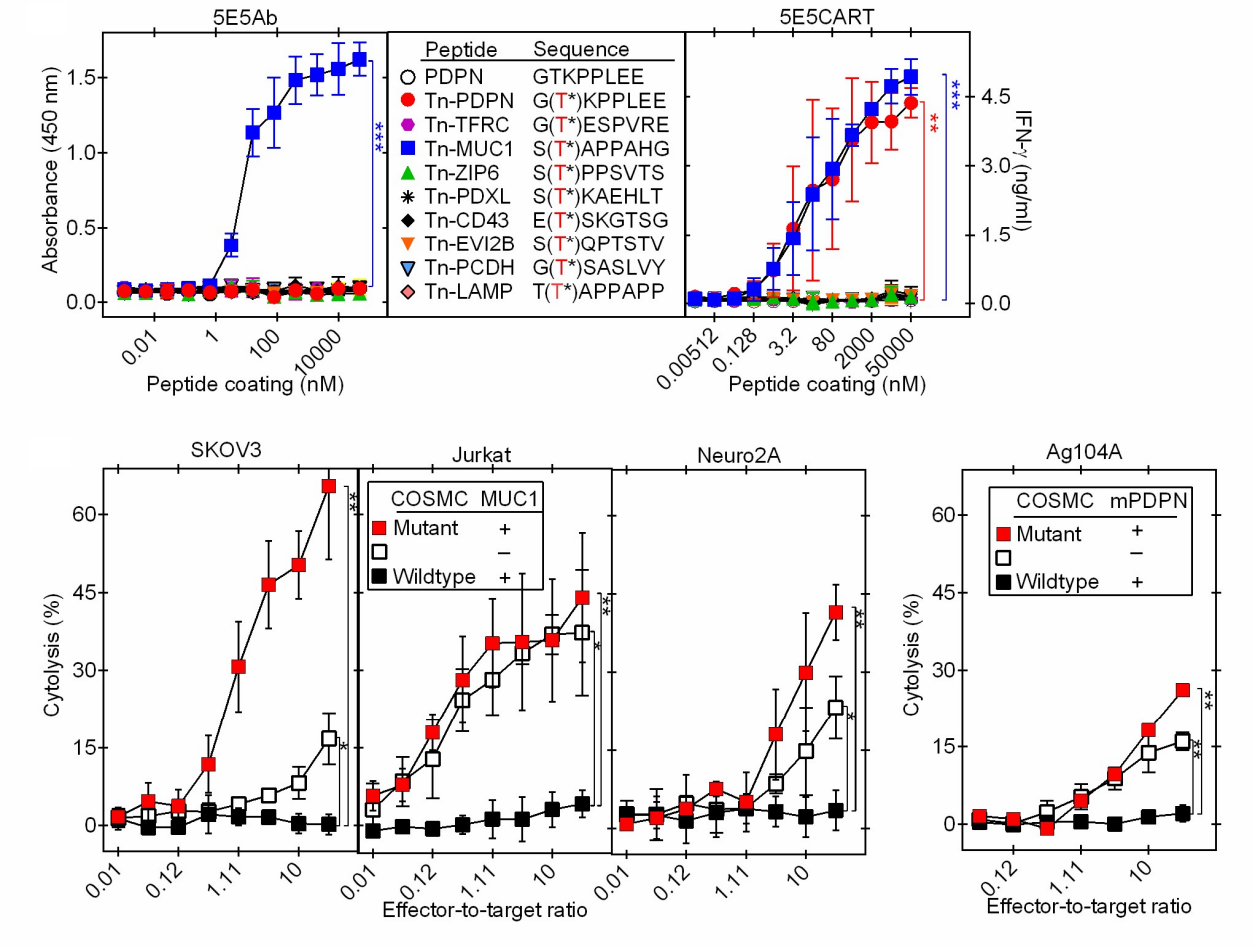

Figure 24. 5E5CART derived from a Tn-MUC1-specific Ab can recognize multiple different Tn-glycopeptide antigens. **Top left:** 5E5Ab is derived from a mouse immunized with Tn-MUC1 and was tested for binding to a panel of different Tn-glycopeptides naturally present in Jurkat cancer cell line. **Top Right:** The activation of 5E5CART in recognition of Tn-glycopeptides found in Jurkat cancer cell line by cytokine release measured by ELISA. **Bottom Left:** 5E5CART cells lysed COSMC-mutant cancers from different cellular background with or without MUC1 expression. **Bottom Left:** 5E5CART cells lysed COSMC-mutant Ag104A tumor with or without mPDPN expression. The statistical significance of the differences between two groups as pointed by the bracket was calculated by Student's t-test. Mean ± SEM, n = 2

– **Discussion:**

My results showed that 237CART recognize COSMC-mutant cancers without murine PDPN expression, while it still retained a preferential reactivity towards Tn-mPDPN as the 237CART activation level was always lower in the absence of murine PDPN. Two complementary explanations present themselves. One is the specificity of 237CAR is shifted from that of the original 237Ab due to the structural difference between the full IgG and the *scFv*. A second explanation is the concentration of multiple targets at the immunological synapse enhanced CART sensitivity to low-density and/or weak-binding mimotopes through the avidity effect (70). For detection of Ab staining by flow cytometry, it generally requires >100 binding per cell to generate meaningful signal. While target lysis by T cells can be mediated by as few as 1–10 TCR, or 100-200 CAR engagements per cell (71). To better understand the mechanism behind the expanded recognition of Tn-glycopeptides by CART cells derived from Tn-glycopeptide-specific Ab, more sensitive binding assays than flow cytometry like Biacore might enhance our understanding about the change in binding affinity of *scFv* compared to that of the original antibody. While only the crystallography of the structure of 237Ab binding to its ligand has been resolved, it would be important to acquire structural studies like crystallography or NMR of 5E5Ab as well to obtain a more comprehensive view about the potential similarities and differences in the mode of binding compared to that of 237Ab.

5. SUMMARY AND PERSPECTIVES

It has previously been shown that 237Ab recognizes the cancer-specific Tn-glycosylated mPDPN on the surface of Ag104A tumor that resulted from a spontaneous loss-of-function mutation of COSMC (44). To take advantage of the exceptional cancer-specificity of 237Ab and the potency of CART to eradicate late-stage cancers (11), the *scFv* of 237Ab was converted into a 2nd generation CAR by fusing the *scFv* with the T-cell signaling and T-cell co-stimulatory signals similar to that has been used for the clinically proven CD19CART cells (**Figure 1**) (11). 237Ab has displayed exclusive specificity in binding to COSMC-mutant cell lines expressing mPDPN. While 237CART cells recognized all COSMC-mutant cell lines tested, the activity was always stronger in the presence Tn-PDPN, and none of the COSMC-wildtype cell lines were able to activate the 237CART cells. These results demonstrated the wide applicability of 237CART towards a broad range of human cancers that are Tn-glycosylated.

It has been shown by crystallography that 237Ab interacts with a 7-AA-residue-long epitope in mPDPN surrounding the Tn-glycosylated Thr^{77} (45). To determine the motif required by 237CART recognition, a panel of chemically synthesized Tn-mPDPN derivatives with Ala replacements was tested for their capability to stimulate 237CART to release IFN-γ. The results demonstrated 237CART can tolerate up to 4 of the 5 C-terminal aa residues replacement into Ala without significantly compromising the activation of 237CART, I further investigated the minimal length of the C-terminal peptide required for 237CART activation. By gradually truncation of the Tn-mPDPN motif from the C-terminal, I found 237CART tolerated the reduction of up to 4 aa residues until the recognition was completely abrogated. Furthermore, a panel of Tn-glycopeptides naturally present in Jurkat (57) were

tested for their recognition by 237CART. Thus, my work revealed that 237CART can recognize multiple different cancer-specific Tn-glycopeptide Ags not predicted by 237Ab binding.

CD19CART has achieved exceptional efficacy in patients with late-stage B-cell leukemia (61). To compare the *in vivo* efficacy of 237CART to that of CD19CART, I employed a 14-day established leukemia model of Jurkat transplanted in NSG mice. Jurkat is a human T-cell leukemia has a spontaneous loss-of-function COSMC mutation (47) and the *Pdpn*-transduced, the COSMC-wildtype-and-CD19-transduced, and the parental Jurkat were transplanted into NSG mice via tail vein injection. Two weeks after the tumor injection, 237CART cells were given via i.p. injection and surprisingly, the treatment achieved long-term disease-free survival in both *Pdpn*-transduced and the parental Jurkat transplanted groups, while the transduction of wildtype COSMC completely abolished the therapeutic efficacy due to the loss of Tn-glycopeptide epitopes from the restored normal *O*-linked glycosylation. The experiment showed the exceptional efficacy of 237CART in treating Jurkat leukemia comparable to that treated by CD19CART. It also has demonstrated the recognition of Tn-glycopeptides other than Tn-mPDPN was sufficient to reject established Jurkat leukemia *in vivo*. I have also tested the efficacy of 237CART cells for the treatment of the parental Jurkat cells as a s.c. transplant in two NSG mice. Regardless the need for repeated dosing on one mouse, the Jurkat as s.c. tumors were completely rejected in both animals. The results encouraged me to further explore the potency of 237CART for treating other cancers including cell lines from solid tumor background.

I first determined whether 237CART could reject SKOV3 tumor which had been reported to be rejected by anti-Her2 CART treatment (62), and found the treatment could only reject

COSMC-mutant SKOV3 in the presence of mPDPN but not without. These data suggested that strong 237CART activation in recognition of ideal cognate Ags like Tn-mPDPN may be required for the rejection of established solid tumors.

Moreover, I determined the efficacy of 237CART for treating a mouse sarcoma, Ag104A, the tumor which stimulated the generation of 237Ab and expresses a high level of Tn-mPDPN (43). However, the 237CART treatment alone barely had any effect to achieve even a temporal regression of the tumor growth. Considering the potential challenges of T cells to penetrate an established solid tumor, I repeated the 237CART treatment of Ag104A at a much earlier stage and found the 237CART treatment could still not repress the growth of a very small (~100 mm^3) Ag104A tumor (**Figure 21**).

Due to the hypothesis that $CD4^+$ T cells may facilitate the insufficient $CD8^+$ T cells to last longer and act stronger, I treated mRLRP9-Ag104A tumor that expresses Tn-glycopeptide antigens that can be targeted by 237CAR-transduced $CD8^+$ T-cell and mRLRP9 presented on MHC class II that can be targeted by 479-H60 TCR-transduced $CD4^+$ T-cell with the combination of $CD8^+$ and $CD4^+$ T-cell treatment. However, I have only observed in two mice limited efficacy of the treatment to only slowed down the tumor growth compared to historical untreated control, the results of which needs to be further validated by more repeats and the comparison to $CD8^+$ or $CD4^+$ T-cell treatment alone. The dramatic differences of the responses to 237CART between Ag104A and SKOV3 COSMC-mutant-mPDPN indicated that some innate features of Ag104A might be compromising the therapeutic efficacy of 237CART in its tumor microenvironment. While I have not found an approach to fully reject the established Ag104A tumor, I collected preliminary evidence suggesting the potential mechanisms of solid tumor resistance to CART treatment. Potentially strategies to optimize CART treatments for

solid tumors include: 1. Selecting homogenously and stably expressed Ags. 2. Optimizing the CAR construct for more durable *in vivo* potency and persistence. 3. Combining the cancer-targeting CART with the stromal-targeting TCR-transduced T-cell to increase the Ag coverage of the tumor and modulate the immune-suppressive cancer microenvironment.

Last but not least, I have tested the general applicability of the expanded cancer-specificity of a CAR derived from a Tn-glycopeptide-specific Ab, and found 5E5, a mAb developed from immunizing mice with Tn-MUC1, also recognized Tn-glycopeptides not predicted by the Ab binding. The observation validates a new paradigm of using a CAR derived from a mAb specific for a particular Tn-glycopeptide for simultaneous targeting a broader range of cancer-specific Tn-glycopeptide antigens. The broadened cancer-reactivity remains safe because of its dependence on the COSMC mutation that is not found in normal tissue. In order to achieve better T cell activation upon recognition of human cancers, the *scFv* of the CARs can be further optimized for better affinity with any particular Tn-glycopeptide that is commonly found in many human cancer types.

REFERENCES:

1. Jazaeri AA, Zsiros E, Amaria RN, Artz AS, Edwards RP, Wenham RM, Slomovitz BM, Walther A, Thomas SS, Chesney JA, et al. Safety and efficacy of adoptive cell transfer using autologous tumor infiltrating lymphocytes (LN-145) for treatment of recurrent, metastatic, or persistent cervical carcinoma. *Journal of Clinical Oncology.* 2019;37(15_suppl):2538-.

2. Sarnaik A, Thomas S, and Davar D. *33rd annual meeting & pre-conference programs of the Society for Immunotherapy of Cancer (SITC 2018)*. 2018.

3. Rosenberg SA, Spiess P, and Lafreniere R. A new approach to the adoptive immunotherapy of cancer with tumor-infiltrating lymphocytes. *Science.* 1986;233(4770):1318-21.

4. Dudley ME, Wunderlich JR, Yang JC, Sherry RM, Topalian SL, Restifo NP, Royal RE, Kammula U, White DE, Mavroukakis SA, et al. Adoptive cell transfer therapy following non-myeloablative but lymphodepleting chemotherapy for the treatment of patients with refractory metastatic melanoma. *J Clin Oncol.* 2005;23(10):2346-57.

5. Rosenberg SA, Packard BS, Aebersold PM, Solomon D, Topalian SL, Toy ST, Simon P, Lotze MT, Yang JC, Seipp CA, et al. Use of tumor-infiltrating lymphocytes and interleukin-2 in the immunotherapy of patients with metastatic melanoma. A preliminary report. *N Engl J Med.* 1988;319(25):1676-80.

6. Leisegang M, Kammertoens T, Uckert W, and Blankenstein T. Targeting human melanoma neoantigens by T cell receptor gene therapy. *J Clin Invest.* 2016;126(3):854-8.

7. Leisegang M, Engels B, Schreiber K, Yew PY, Kiyotani K, Idel C, Arina A, Duraiswamy J, Weichselbaum RR, Uckert W, et al. Eradication of Large Solid Tumors by Gene Therapy with a T-Cell Receptor Targeting a Single Cancer-Specific Point Mutation. *Clin Cancer Res.* 2016;22(11):2734-43.

8. Khong HT, Wang QJ, and Rosenberg SA. Identification of multiple antigens recognized by tumor-infiltrating lymphocytes from a single patient: tumor escape by antigen loss and loss of MHC expression. *J Immunother.* 2004;27(3):184-90.

9. Eshhar Z, Waks T, Gross G, and Schindler DG. Specific activation and targeting of cytotoxic lymphocytes through chimeric single chains consisting of antibody-binding domains and the gamma or zeta subunits of the immunoglobulin and T-cell receptors. *Proc Natl Acad Sci U S A.* 1993;90(2):720-4.

10. Sadelain M, Brentjens R, and Riviere I. The basic principles of chimeric antigen receptor design. *Cancer Discov.* 2013;3(4):388-98.

11. Porter DL, Levine BL, Kalos M, Bagg A, and June CH. Chimeric antigen receptor-modified T cells in chronic lymphoid leukemia. *N Engl J Med.* 2011;365(8):725-33.

12. Morgan RA, Yang JC, Kitano M, Dudley ME, Laurencot CM, and Rosenberg SA. Case report of a serious adverse event following the administration of T cells transduced with a chimeric antigen receptor recognizing ERBB2. *Mol Ther.* 2010;18(4):843-51.

13. Hegde M, Mukherjee M, Grada Z, Pignata A, Landi D, Navai SA, Wakefield A, Fousek K, Bielamowicz K, Chow KK, et al. Tandem CAR T cells targeting HER2 and IL13Ralpha2 mitigate tumor antigen escape. *J Clin Invest.* 2016;126(8):3036-52.

14. Roybal KT, Rupp LJ, Morsut L, Walker WJ, McNally KA, Park JS, and Lim WA. Precision Tumor Recognition by T Cells With Combinatorial Antigen-Sensing Circuits. *Cell.* 2016;164(4):770-9.

15. Brown CE, Aguilar B, Starr R, Yang X, Chang WC, Weng L, Chang B, Sarkissian A, Brito A, Sanchez JF, et al. Optimization of IL13Ralpha2-Targeted Chimeric Antigen Receptor T Cells for Improved Anti-tumor Efficacy against Glioblastoma. *Mol Ther.* 2018;26(1):31-44.

16. Choi BD, Suryadevara CM, Gedeon PC, Herndon JE, 2nd, Sanchez-Perez L, Bigner DD, and Sampson JH. Intracerebral delivery of a third generation EGFRvIII-specific chimeric antigen receptor is efficacious against human glioma. *J Clin Neurosci.* 2014;21(1):189-90.

17. Hakomori S. Tumor-associated carbohydrate antigens defining tumor malignancy: basis for development of anti-cancer vaccines. *Adv Exp Med Biol.* 2001;491(369-402.

18. Astronomo RD, and Burton DR. Carbohydrate vaccines: developing sweet solutions to sticky situations? *Nat Rev Drug Discov.* 2010;9(4):308-24.

19. Sorensen AL, Reis CA, Tarp MA, Mandel U, Ramachandran K, Sankaranarayanan V, Schwientek T, Graham R, Taylor-Papadimitriou J, Hollingsworth MA, et al. Chemoenzymatically synthesized multimeric Tn/STn MUC1 glycopeptides elicit cancer-specific anti-MUC1 antibody responses and override tolerance. *Glycobiology.* 2006;16(2):96-107.

20. Roulois D, Gregoire M, and Fonteneau JF. MUC1-specific cytotoxic T lymphocytes in cancer therapy: induction and challenge. *Biomed Res Int.* 2013;2013(871936.

21. Roth Z, Yehezkel G, and Khalaila I. Identification and quantification of protein glycosylation. *International Journal of Carbohydrate Chemistry.* 2012;2012.

22. Hang HC, and Bertozzi CR. The chemistry and biology of mucin-type O-linked glycosylation. *Bioorg Med Chem.* 2005;13(17):5021-34.

23. Ten Hagen KG, Fritz TA, and Tabak LA. All in the family: the UDP-GalNAc:polypeptide N-acetylgalactosaminyltransferases. *Glycobiology.* 2003;13(1):1R-16R.

24. Tarp MA, and Clausen H. Mucin-type O-glycosylation and its potential use in drug and vaccine development. *Biochim Biophys Acta.* 2008;1780(3):546-63.

25. Miwa HE, Gerken TA, Jamison O, and Tabak LA. Isoform-specific O-glycosylation of osteopontin and bone sialoprotein by polypeptide N-acetylgalactosaminyltransferase-1. *J Biol Chem.* 2010;285(2):1208-19.

26. Pratt MR, Hang HC, Ten Hagen KG, Rarick J, Gerken TA, Tabak LA, and Bertozzi CR. Deconvoluting the functions of polypeptide N-alpha-acetylgalactosaminyltransferase family members by glycopeptide substrate profiling. *Chem Biol.* 2004;11(7):1009-16.

27. Springer GF. T and Tn, general carcinoma autoantigens. *Science.* 1984;224(4654):1198-206.

28. Springer GF. Immunoreactive T and Tn epitopes in cancer diagnosis, prognosis, and immunotherapy. *J Mol Med (Berl).* 1997;75(8):594-602.

29. Ju T, Otto VI, and Cummings RD. The Tn antigen-structural simplicity and biological complexity. *Angew Chem Int Ed Engl.* 2011;50(8):1770-91.

30. Ju T, and Cummings RD. A unique molecular chaperone Cosmc required for activity of the mammalian core 1 beta 3-galactosyltransferase. *Proc Natl Acad Sci U S A.* 2002;99(26):16613-8.

31. Ju T, Lanneau GS, Gautam T, Wang Y, Xia B, Stowell SR, Willard MT, Wang W, Xia JY, Zuna RE, et al. Human tumor antigens Tn and sialyl Tn arise from mutations in Cosmc. *Cancer Res.* 2008;68(6):1636-46.

32. Brooks SA, Carter TM, Bennett EP, Clausen H, and Mandel U. Immunolocalisation of members of the polypeptide N-acetylgalactosaminyl transferase (ppGalNAc-T) family is consistent with biologically relevant altered cell surface glycosylation in breast cancer. *Acta Histochem.* 2007;109(4):273-84.

33. Gill DJ, Clausen H, and Bard F. Location, location, location: new insights into O-GalNAc protein glycosylation. *Trends Cell Biol.* 2011;21(3):149-58.

34. Guda K, Moinova H, He J, Jamison O, Ravi L, Natale L, Lutterbaugh J, Lawrence E, Lewis S, Willson JK, et al. Inactivating germ-line and somatic mutations in polypeptide N-acetylgalactosaminyltransferase 12 in human colon cancers. *Proc Natl Acad Sci U S A.* 2009;106(31):12921-5.

35. Guo JM, Chen HL, Wang GM, Zhang YK, and Narimatsu H. Expression of UDP-GalNAc:polypeptide N-acetylgalactosaminyltransferase-12 in gastric and colonic cancer cell lines and in human colorectal cancer. *Oncology.* 2004;67(3-4):271-6.

36. Park JH, Katagiri T, Chung S, Kijima K, and Nakamura Y. Polypeptide N-acetylgalactosaminyltransferase 6 disrupts mammary acinar morphogenesis through O-glycosylation of fibronectin. *Neoplasia.* 2011;13(4):320-6.

37. Taniuchi K, Cerny RL, Tanouchi A, Kohno K, Kotani N, Honke K, Saibara T, and Hollingsworth MA. Overexpression of GalNAc-transferase GalNAc-T3 promotes pancreatic cancer cell growth. *Oncogene.* 2011;30(49):4843-54.

38. Mi R, Song L, Wang Y, Ding X, Zeng J, Lehoux S, Aryal RP, Wang J, Crew VK, van Die I, et al. Epigenetic silencing of the chaperone Cosmc in human leukocytes expressing tn antigen. *J Biol Chem.* 2012;287(49):41523-33.

39. Radhakrishnan P, Dabelsteen S, Madsen FB, Francavilla C, Kopp KL, Steentoft C, Vakhrushev SY, Olsen JV, Hansen L, Bennett EP, et al. Immature truncated O-glycophenotype of cancer directly induces oncogenic features. *Proc Natl Acad Sci U S A.* 2014;111(39):E4066-75.

40. Ju T, and Cummings RD. Protein glycosylation: chaperone mutation in Tn syndrome. *Nature.* 2005;437(7063):1252.

41. Bird GW. Plant and other agglutinins in the study of some human erythrocyte membrane anomalies. *Ann N Y Acad Sci.* 1974;234(0):129-44.

42. Thurnher M, Rusconi S, and Berger EG. Persistent repression of a functional allele can be responsible for galactosyltransferase deficiency in Tn syndrome. *J Clin Invest.* 1993;91(5):2103-10.

43. Ward PL, Koeppen H, Hurteau T, and Schreiber H. Tumor antigens defined by cloned immunological probes are highly polymorphic and are not detected on autologous normal cells. *J Exp Med.* 1989;170(1):217-32.

44. Schietinger A, Philip M, Yoshida BA, Azadi P, Liu H, Meredith SC, and Schreiber H. A mutant chaperone converts a wild-type protein into a tumor-specific antigen. *Science.* 2006;314(5797):304-8.

45. Brooks CL, Schietinger A, Borisova SN, Kufer P, Okon M, Hirama T, Mackenzie CR, Wang LX, Schreiber H, and Evans SV. Antibody recognition of a unique tumor-specific glycopeptide antigen. *Proc Natl Acad Sci U S A.* 2010;107(22):10056-61.

46. Monach PA, Meredith SC, Siegel CT, and Schreiber H. A unique tumor antigen produced by a single amino acid substitution. *Immunity.* 1995;2(1):45-59.

47. Posey AD, Jr., Schwab RD, Boesteanu AC, Steentoft C, Mandel U, Engels B, Stone JD, Madsen TD, Schreiber K, Haines KM, et al. Engineered CAR T Cells Targeting the Cancer-Associated Tn-Glycoform of the Membrane Mucin MUC1 Control Adenocarcinoma. *Immunity.* 2016;44(6):1444-54.

48. Olmsted JB, Carlson K, Klebe R, Ruddle F, and Rosenbaum J. Isolation of microtubule protein from cultured mouse neuroblastoma cells. *Proc Natl Acad Sci U S A.* 1970;65(1):129-36.

49. Chen W, Zarnitsyna VI, Sarangapani KK, Huang J, and Zhu C. Measuring Receptor-Ligand Binding Kinetics on Cell Surfaces: From Adhesion Frequency to Thermal Fluctuation Methods. *Cell Mol Bioeng.* 2008;1(4):276-88.

50. Huse M, Klein LO, Girvin AT, Faraj JM, Li QJ, Kuhns MS, and Davis MM. Spatial and temporal dynamics of T cell receptor signaling with a photoactivatable agonist. *Immunity.* 2007;27(1):76-88.

51. Edelstein AD, Tsuchida MA, Amodaj N, Pinkard H, Vale RD, and Stuurman N. Advanced methods of microscope control using muManager software. *J Biol Methods.* 2014;1(2).

52. Huang J, Zarnitsyna VI, Liu B, Edwards LJ, Jiang N, Evavold BD, and Zhu C. The kinetics of two-dimensional TCR and pMHC interactions determine T-cell responsiveness. *Nature.* 2010;464(7290):932-6.

53. Huang J, Edwards LJ, Evavold BD, and Zhu C. Kinetics of MHC-CD8 interaction at the T cell membrane. *J Immunol.* 2007;179(11):7653-62.

54. Zhang T, He X, Tsang TC, and Harris DT. Transgenic TCR expression: comparison of single chain with full-length receptor constructs for T-cell function. *Cancer Gene Ther.* 2004;11(7):487-96.

55. Engels B, Cam H, Schuler T, Indraccolo S, Gladow M, Baum C, Blankenstein T, and Uckert W. Retroviral vectors for high-level transgene expression in T lymphocytes. *Hum Gene Ther.* 2003;14(12):1155-68.

56. Gee KR, Brown KA, Chen WN, Bishop-Stewart J, Gray D, and Johnson I. Chemical and physiological characterization of fluo-4 Ca(2+)-indicator dyes. *Cell Calcium.* 2000;27(2):97-106.

57. Steentoft C, Vakhrushev SY, Vester-Christensen MB, Schjoldager KT, Kong Y, Bennett EP, Mandel U, Wandall H, Levery SB, and Clausen H. Mining the O-glycoproteome using zinc-finger nuclease-glycoengineered SimpleCell lines. *Nat Methods.* 2011;8(11):977-82.

58. Glazer AN. On the prevalence of "nonspecific" binding at the specific binding sites of globular proteins. *Proc Natl Acad Sci U S A.* 1970;65(4):1057-63.

59. Richards FF, Konigsberg WH, Rosenstein RW, and Varga JM. On the specificity of antibodies. *Science.* 1975;187(4172):130-7.

60. Bedoya F, Frigault MJ, and Maus MV. The Flipside of the Power of Engineered T Cells: Observed and Potential Toxicities of Genetically Modified T Cells as Therapy. *Mol Ther.* 2017;25(2):314-20.

61. June CH, and Sadelain M. Chimeric Antigen Receptor Therapy. *N Engl J Med.* 2018;379(1):64-73.

62. Textor A, Listopad JJ, Wuhrmann LL, Perez C, Kruschinski A, Chmielewski M, Abken H, Blankenstein T, and Charo J. Efficacy of CAR T-cell therapy in large tumors relies upon stromal targeting by IFNgamma. *Cancer Res.* 2014;74(23):6796-805.

63. Purbhoo MA, Irvine DJ, Huppa JB, and Davis MM. T cell killing does not require the formation of a stable mature immunological synapse. *Nat Immunol.* 2004;5(5):524-30.

64. Huang J, Brameshuber M, Zeng X, Xie J, Li QJ, Chien YH, Valitutti S, and Davis MM. A single peptide-major histocompatibility complex ligand triggers digital cytokine secretion in CD4(+) T cells. *Immunity.* 2013;39(5):846-57.

65. Han A, Glanville J, Hansmann L, and Davis MM. Linking T-cell receptor sequence to functional phenotype at the single-cell level. *Nat Biotechnol.* 2014;32(7):684-92.

66. Schietinger A, Philip M, Liu RB, Schreiber K, and Schreiber H. Bystander killing of cancer requires the cooperation of CD4(+) and CD8(+) T cells during the effector phase. *J Exp Med.* 2010;207(11):2469-77.

67. Bos R, and Sherman LA. CD4+ T-cell help in the tumor milieu is required for recruitment and cytolytic function of CD8+ T lymphocytes. *Cancer Res.* 2010;70(21):8368-77.

68. Rafiq S, Yeku OO, Jackson HJ, Purdon TJ, van Leeuwen DG, Drakes DJ, Song M, Miele MM, Li Z, Wang P, et al. Targeted delivery of a PD-1-blocking scFv by CAR-T cells enhances anti-tumor efficacy in vivo. *Nat Biotechnol.* 2018;36(9):847-56.

69. Tarp MA, Sorensen AL, Mandel U, Paulsen H, Burchell J, Taylor-Papadimitriou J, and Clausen H. Identification of a novel cancer-specific immunodominant glycopeptide epitope in the MUC1 tandem repeat. *Glycobiology.* 2007;17(2):197-209.

70. Stone JD, Aggen DH, Schietinger A, Schreiber H, and Kranz DM. A sensitivity scale for targeting T cells with chimeric antigen receptors (CARs) and bispecific T-cell Engagers (BiTEs). *Oncoimmunology.* 2012;1(6):863-73.

71. Harris DT, and Kranz DM. Adoptive T Cell Therapies: A Comparison of T Cell Receptors and Chimeric Antigen Receptors. *Trends Pharmacol Sci.* 2016;37(3):220-30.